Point-by-point response to referees

We thank the reviewer for the insightful and constructive comments. We have made point-by-point responses and/or revisions according to your suggestions and instructions. We recall the comments of the reviewer in black, followed by our reply in blue.

Please note that we have rerun the simulations involving RUN(3) as replied to the comment #3 from referee #2, and all the figures in the manuscript have been revised accordingly.

All the lines in our responses refer to the line numbers in the marked-up manuscript, which shows all the changes and is appended at the end of this response.

Responses to Referee #1

Anonymous Referee #1

Received and published: 15 September 2020

The authors systematically evaluated the effects of different physical processes and associated parameterization options on Noah-MP simulated soil temperature at a permafrost site over the Tibetan Plateau. The manuscript is generally well-written and well-structured. Before it can be considered for potential publication, I have a few comments for the authors to consider.

Major comment:

1. I am not convinced why the authors did not test the snow-related processes and parameterizations, such as snow albedo and rain-snow partitioning schemes. These processes along with the snow cover formulation in Noah-MP will affect surface heat fluxes and energy balance, which can potentially affect soil temperature evolution below snowpack. Particularly, the authors found that Noah-MP generally underestimates the soil temperature during the cold season, which could partially be related to snowpack simulations. The authors also did not tell the readers that what

parameterization schemes they used for snow albedo and partitioning processes.

Moreover, a recent study over Tibetan Plateau (Jiang et al., 2020, https://agupubs.onlinelibrary.wiley.com/doi/abs/10.1029/2020JD032674) showed that the processes already tested by the authors here along with the snow cover formulation can significantly affect snowpack simulations, which could further affect soil conditions. Thus, it is likely that the processes the authors tested can indirectly affect soil conditions through modifying snowpack. I suggest the authors add some discussions on this aspect and include some quick tests for snow-related processes if possible.

Response: Thank you for your constructive suggestion! In the revised manuscript, we have conducted an ensemble of 41472 (= 6912*2*3) experiments to test the performance of Noah-MP in simulating snow processes. Results show that Noah-MP extremely overestimates the albedo and thus induces great cold bias in soil temperature. Detailed results and discussions are illustrated in the newly added Sec. 3.1.1 and Sec. 4.1, respectively.

In addition, snow process is not considered by setting the snow fraction in precipitation to zero in this study. Since no snow cover in the ground, the ground albedo equals the soil albedo. We have added some explanations in lines 164-167: "For practical purpose, the ALB and SNF processes were not considered by setting the snow fraction in precipitation to zero. Since no snow cover in the ground, the ground albedo equals the soil albedo".

Minor comments:

1. Line 108: "depth" -> "depths".

Response: Revised as suggested.

2. Line 170: Please give some details on how the soil column was discretized, e.g., how many soil layers, the thickness of each layer, etc.

Response: The details of each layer are listed in the supplementary file as Table S1:

Table S1 Soil discretization scheme and soil particle fraction in this study.

Layer	Z_i	ΔZ_i	$Z_{h,i}$	Sand (%)	Silt (%)	Clay (%)
1	0.010	0.020	0.020			
2	0.040	0.040	0.060	85.48	12.59	1.93
3	0.090	0.060	0.120			
4	0.160	0.080	0.200	83.51	13.57	2.92
5	0.260	0.120	0.320	81.15	15.58	3.27
6	0.400	0.160	0.480	86.62	11.16	2.22
7	0.580	0.200	0.680	78.73	18.06	3.21
8	0.800	0.240	0.920	88.12	8.98	2.90
9	1.060	0.280	1.200	95.00	3.00	2.00
10	1.360	0.320	1.520			
11	1.700	0.360	1.880	92.50	4.00	3.50
12	2.080	0.400	2.280			
13	2.500	0.440	2.720	90.00	5.00	5.00
14	2.990	0.540	3.260			
15	3.580	0.640	3.900			
16	4.270	0.740	4.640			
17	5.060	0.840	5.480			
18	5.950	0.940	6.420	68.00	20.00	12.00
19	6.940	1.040	7.460			
20	7.980	1.040	8.500			

Layer node depth (Z_i), thickness (ΔZ_i), and depth at layer interface ($Z_{h,i}$) for default soil column. All in meters.

Accordingly, we revised the sentences in lines 174-186 as "The soil hydraulic parameters, including the porosity, saturated hydraulic conductivity, hydraulic potential, the Clapp-Hornberger parameter b, field capacity, wilt point, and saturated soil water diffusivity, were determined using the pedotransfer functions proposed by Hillel (1980), Cosby et al. (1984), and Wetzel and Chang (1987) (Equations S1-S7), in which the sand and clay percentages were based on Hu et al., (2017) (Table S1). In addition, the simulation depth was extended to 8.0 m to cover the active layer thickness of the QTP. The soil column was discretized into 20 layers, whose depths follow the default scheme in CLM 5.0 (Table S1, Lawrence et al., 2018). Due to the inexact match between observed and simulated depths, the simulations at 4cm, 26cm, 80cm, 136cm, 208cm and 299cm were compared with the observations at 5cm, 25cm, 70cm, 140cm, 220cm and 300cm, respectively. A 30-year spin-up was conducted in every simulation to reach

equilibrium soil states.".

3. Line 189: What is "Si"?

Response: Sorry for the typo. It should be $\Delta\overline{RMSE}$, which has been corrected in line 203.

4. What is the model timestep in the simulations in this study?

Response: The model was driven by 1-hr-interval atmospheric forcing data, which has been described in lines 138-144: "The atmospheric forcing data, including wind speed/direction, air temperature/relative humidity/pressure, downward shortwave/longwave radiation, and precipitation, were used to drive the model. These variables above were measured at a height of 2 m and covered the period from August 10, 2010 to August 10, 2012 (Beijing time) with a temporal resolution of 1 hour. Daily soil temperature and moisture at depths of 5cm, 25cm, 70cm, 140cm, 220cm and 300cm from October 1, 2010 to September 30, 2011 (Beijing time) were utilized to validate the simulation results."

5. Section 4.3: The authors only tested the model performance at one site. So to what extent their conclusions can be extended to other Tibetan Plateau areas?

Response: Thanks for this review. We agree that further work is required in the future as discussed in Sec. 4.4. In this study, our main goal is to provide a reference for simulating permafrost state on the Tibet Plateau. However, before the whole Tibetan Plateau can be investigated, it is necessary to conduct such study at the site scale.

We believe the conclusion of the cold bias of Noah-MP in the Tibetan Plateau and the possible reasons are of high reliability. The study site is a typical permafrost site on the plateau with semiarid climate (Li et al., 2019), filmy and discontinuous snow cover (Che et al., 2019), sparse grassland (Yao et al., 2011), coarse soil (Wu and Nan, 2016; He et al., 2019), and thick active layer (Luo et al., 2016), which are common features in the permafrost regions of the plateau. In addition, such underestimations and the

inabilities of producing the snow depth, diurnal Z_{0h} and frozen soil thermal conductivity are widely reported in many state-of-the-art land surface models as discussed in Sec. 4.1 and 4.2.

In addition, the sensitivity analysis and optimal configuration of the physical processes in this study could contribute to better understand the land surface processes and provide practical guidelines for permafrost modeling at least in the permafrost areas with similar conditions on the plateau. Relevant methodologies could be generalized to other regions using the proposed approaches.

To be more unbiased and objective, we added some descriptions about the study site, and the new version in lines 126-131 are: "Tanggula observation station (TGL) lies in the continuous permafrost regions of Tanggula Mountain, central QTP (33.07°N, 91.93°E, Alt.: 5,100 m a.s.l; Fig. 1). This site a typical permafrost site on the plateau with sub-frigid and semiarid climate (Li et al., 2019), filmy and discontinuous snow cover (Che et al., 2019), sparse grassland (Yao et al., 2011), coarse soil (Wu and Nan, 2016; He et al., 2019), and thick active layer (Luo et al., 2016), which are common features in the permafrost regions of the plateau.".

And the perspective part (section 4.4) in lines 603-612 are rephrased as: "This study analyzed the characteristics and general behaviors of each parameterization scheme of Noah-MP at a typical permafrost site on the QTP, hoping to provide a reference for simulating permafrost state on the QTP. We identified the systematic overestimation of snow cover and cold bias in Noah-MP, and discussed the possible sources of error. Relevant results and methodologies can be practical guidelines for improving the parameterizations of physical processes and testing their uncertainties towards near-surface permafrost modeling on the plateau. Although the site we selected may be representative for the typical environment on the plateau, continued investigation with a broad spectrum of climate and environmental conditions is required to make a general conclusion at regional scale.".

References:

Che, T., Hao, X., Dai, L., Li, H., Huang, X., and Xiao, L.: Snow cover variation and its impacts over the Qinghai-Tibet Plateau, Bull. Chin. Acad. Sci., 34, 1247-1253, https://doi.org/10.16418/j.issn.1000-3045.2019.11.007, 2019.

He, K., Sun, J., and Chen, Q.: Response of climate and soil texture to net primary productivity and precipitation-use efficiency in the Tibetan Plateau, Pratacultural Science, 36(4), 1053–1065. https://doi.org/10.11829/j.issn.1001-0629.2019-0036, 2019.

Li, R., Zhao, L., Wu, T., Wang, Q. X., Ding, Y., Yao, J., Wu, X., Hu, G., Xiao, Y., Du, Y., Zhu, X., Qin, Y., Shuhua, Y., Bai, R., Erji, D., Liu, G., Zou, D., Yongping, Q., and Shi, J.: Soil thermal conductivity and its influencing factors at the Tanggula permafrost region on the Qinghai–Tibet Plateau, Agric. For. Meteor., 264, 235-246, https://doi.org/10.1016/j.agrformet.2018.10.011, 2019.

Luo, D., Wu, Q., Jin, H., Marchenko, S., Lyu, L., and Gao, S.: Recent changes in the active layer thickness across the northern hemisphere, Environ. Earth Sci., 75(7), 555. https://doi.org/10.1007/s12665-015-5229-2, 2016.

Wu, X., and Nan, Z.: A multilayer soil texture dataset for permafrost modeling over Qinghai-Tibetan Plateau. Paper presented at 2016 IEEE International Geoscience and Remote Sensing Symposium (IGARSS), Beijing, China. https://doi.org/10.1109/IGARSS.2016.7730283, 2016.

Yao, J., Zhao, L., Gu, L., Qiao, Y., and Jiao, K.: The surface energy budget in the permafrost region of the Tibetan Plateau, Atmos. Res., 102, 394-407, https://doi.org/https://doi.org/10.1016/j.atmosres.2011.09.001, 2011.

Anonymous Referee #2

Received and published: 13 October 2020

It's my pleasure to review gmd-2020-142 "Assessing the simulated soil thermal regime from Noah-MP LSM v1.1 for near-surface permafrost modeling on the Qinghai-Tibet Plateau" by Li et al. The authors evaluate the performance of Noah-MP in simulating soil temperature on a permafrost site over the Tibetan Plateau. There are many additional work need to be done before this paper can be accepted.

1. I note that there is a paper recently published by the same author to improve the performance of Noah-MP simulations on the same site. It will be interesting the authors firstly add their improvements, and then design more numerical experiments to test the uncertainties of different parameterization options.

Response: Thanks for this comment. The recently published work you mentioned only tested and augmented one selected combination of Noah-MP options. However, this study investigated the general performance and sensitivity of <u>original Noah-MP</u> model with <u>all possible combinations</u>, hoping to provide a reference for simulating permafrost state on the Tibet Plateau. The augmentation work is another big issue and out of scope of this paper. We choose not to add the suggested experiments, but highlight the continued efforts to augment the parameterizations of physical processes and test their uncertainties in the future in lines 603-612:

"This study analyzed the characteristics and general behaviors of each parameterization scheme of Noah-MP at a typical permafrost site on the QTP, hoping to provide a reference for simulating permafrost state on the QTP. We identified the systematic overestimation of snow cover and cold bias in Noah-MP, and discussed the possible sources of error. Relevant results and methodologies can be practical guidelines for improving the parameterizations of physical processes and testing their uncertainties towards near-surface permafrost modeling on the plateau. Although the site we selected may be representative for the typical environment on the plateau, continued

investigation with a broad spectrum of climate and environmental conditions is required to make a general conclusion at regional scale."

With these revisions, we believe the potential readers can understand that our study aims to test the performance of the original Noah-MP, while future work is needed at the plateau scale.

Since one additional site, soil moisture and snow measurements are available, the authors are suggested to also use these measurements to test the Noah-MP's performance. For the frozen soil, the soil moisture and soil temperature are fully coupled, which are also affected by the snow process, so it's also important to evaluate the performance of Noah-MP in simulating these variables.

Response: We agree that add more sites would strengthen our conclusions. However, we realized that this will make our manuscript very long, and it is difficult to descript the results due to the different environmental factors among the sites. Our main goal is to provide a reference for simulating permafrost state on the Tibet Plateau. We tried our best to make this manuscript concise. Therefore, we would rather focus on one site, and it would be easier for potential readers to understand the core ideas.

We realized that potential readers may wonder why we did not assess the model using more data. To be clear, we explained this in the revised version in lines 603-612 as follows: "This study analyzed the characteristics and general behaviors of each parameterization scheme of Noah-MP at a typical permafrost site on the QTP, hoping to provide a reference for simulating permafrost state on the QTP. We identified the systematic overestimation of snow cover and cold bias in Noah-MP, and discussed the possible sources of error. Relevant results and methodologies can be practical guidelines for improving the parameterizations of physical processes and testing their uncertainties towards near-surface permafrost modeling on the plateau. Although the site we selected may be representative for the typical environment on the plateau, continued investigation with a broad spectrum of climate and environmental conditions

is required to make a general conclusion at regional scale.".

To be more unbiased and objective, we added more descriptions about the study site, in lines 126-131: "Tanggula observation station (TGL) lies in the continuous permafrost regions of Tanggula Mountain, central QTP (33.07°N, 91.93°E, Alt.: 5,100 m a.s.l; Fig. 1). This site a typical permafrost site on the plateau with sub-frigid and semiarid climate (Li et al., 2019), filmy and discontinuous snow cover (Che et al., 2019), sparse grassland (Yao et al., 2011), coarse soil (Wu and Nan, 2016; He et al., 2019), and thick active layer (Luo et al., 2016), which are common features in the permafrost regions of the plateau.".

With these revisions, we believe the potential readers can understand our main findings. We keep the manuscript not too lengthy.

● About snow

As the reply to Referee #1, we conducted 41472 simulations to test the performance of Noah-MP in simulating snow cover. Similar with the recently published paper you mentioned (Li et al., 2020), ground albedo was used to roughly reflect the snow events. Our results show that Noah-MP extremely overestimates the albedo and thus induces great cold bias in soil temperature. Detailed results and discussions are illustrated in the newly added Sec. 3.1.1 and Sec. 4.1, respectively.

● About soil moisture

We checked the performance of Noah-MP in simulating soil liquid water (SLW) in the revised manuscript. Results show that the Noah-MP model generally underestimates soil moisture across the profile. The RUN process dominates the SLW simulation in comparison of the very limited impacts of all other physical processes. Detailed results can be found in lines Sec. 3.1.2 and Sec. 3.2.2.

2. Since the snow process is also important for permafrost soil temperature simulations,

it's suggested to also consider the impact of ALB and SNF options.

Response: In the revised manuscript, we firstly checked the performance of Noah-MP for snow simulation and its impacts on soil temperature by considering the ALB and SNF options. Results showed that Noah-MP greatly overestimates snow cover both in magnitude and duration, inducing huge cold bias and large uncertainties in soil temperatures. However, our in-situ measurements and other studies show that snow cover has a very limited influence on soil temperature. Given the poor simulation of Noah-MP for snow cover and the weak impact of snow on soil temperature in reality, we did not consider the snow process in the following parts.

Detailed results and discussions are illustrated in the newly added Sec. 3.1.1 and Sec. 4.1, respectively.

3. It's also suggested to evaluate the performance of Noah-MP for frozen (e.g. October-April) and thawed (e.g. May-September) soil conditions separately. Because it's very strange to me that the impact of RUN is so important for the soil temperature simulations.

Response: We firstly apologize for the wrong coding when modifying the default Noah-MP to consider the vertical heterogeneity in the soil profile. In the wrong version, the maximum infiltration rate in RUN(3) was calculated as a function of all the soil layers (up to 8m in this study). Due to the existence of permafrost below 3m at the study site, the calculated infiltration rate is extremely small, resulting in small soil moisture of RUN(3) (Figure S1 in previous manuscript) and thus great influence degree of RUN process (Figure 3 in previous manuscript).

Following the default Noah-MP, we have rewritten the infiltration rate in RUN(3) as a function of the soil layers no more than 2m. Based on this, we reassessed the performance of Noah-MP for frozen and thawed soil conditions.

However, the main conclusion is consistent with previous manuscript except the

declined influence of RUN process on soil temperature simulation. We have rewritten the main conclusions in lines 640-659 as:

(1) "Noah-MP model tends to overestimate snow cover and thus largely underestimate soil temperature in the permafrost regions of the QTP. Systematic cold bias and large uncertainties of soil temperature still exist after removing the snow processes, particularly at the deep layers and during the cold season. This is largely due to the imperfect model structure with regard to the roughness length for heat and soil thermal conductivity.

(2) Soil temperature is dominated by the surface layer drag coefficient (SFC) while largely influenced by runoff and groundwater (RUN). Other physical processes have little impact on ST simulation, among which VEG, RAD, and STC are more influential on shallow ST, while FRZ, INF and TBOT have greater impacts on deep ST. In addition, CRS and BTR do not significantly affect the simulation results.

(3) The best scheme combination for permafrost simulation are as follows: VEG (table LAI, calculated vegetation fraction), CRS (Jarvis), BTR (Noah), RUN (BATS), SFC (Chen97), RAD (zero canopy gap), FRZ (variant freezing-point depression), INF (hydraulic parameters defined by soil moisture), TBOT (ST at 8 m), STC (semi-implicit)."

4.Detailed information is needed for the following descriptions "The soil 164 hydraulic parameters, including the porosity, saturated hydraulic conductivity, hydraulic potential, the Clapp-Hornberger parameter b, field capacity, wilt point, and saturated soil water diffusivity, were determined using the pedotransfer functions proposed by Hillel (1980), Cosby et al. (1984), and Wetzel and Chang (1987), in which the sand and clay percentages were based on Hu et al., (2017). In addition, the simulation depth was extended to 8.0 m to cover the active layer thickness of the QTP. The soil column was discretized following the default scheme in CLM 5.0 (Lawrence et al., 2018)."

Response: We have added the details of the pedotransfer functions, the discretization scheme of soil column, and the soil particle fractions in the supplementary file:

The soil hydraulic parameters of each layer, including the porosity (θ_s), saturated hydraulic conductivity (K_s), hydraulic potential (ψ_s), the Clapp-Hornberger parameter (b), field capacity (θ_{ref}), wilt point (θ_w), and saturated soil water diffusivity (D_s), were determined using the pedotransfer functions proposed by Hillel (1980), Cosby et al. (1984), and Wetzel and Chang (1987):

$$\theta_s = 0.489 - 0.00126(\%sand) \tag{S1}$$

$$K_s = 7.0556 \times 10^{-6.884 + 0.0153(\%sand)} \tag{S2}$$

$$\psi_s = -0.01 \times 10^{1.88 - 0.0131(\%sand)} \tag{S3}$$

$$b = 2.91 + 0.159(\%clay) \tag{S4}$$

$$\theta_{ref} = \theta_s \left[\frac{1}{3} + \frac{2}{3} \left(\frac{5.79 \times 10^{-9}}{K_s} \right)^{1/(2b+3)} \right] \tag{S5}$$

$$\theta_w = 0.5\theta_s \left(\frac{-200}{\psi_s} \right)^{-1/b} \tag{S6}$$

$$D_s = b \cdot K_s \cdot \left(\frac{\psi_s}{\theta_s} \right) \tag{S7}$$

where $\%sand$ and $\%clay$ represent the percentage (%) of sand and clay content in soil, respectively.

Table S1 Soil discretization scheme and soil particle fraction in this study.

Layer	Z_i	ΔZ_i	$Z_{h,i}$	Sand (%)	Silt (%)	Clay (%)
1	0.010	0.020	0.020			
2	0.040	0.040	0.060	85.48	12.59	1.93
3	0.090	0.060	0.120			
4	0.160	0.080	0.200	83.51	13.57	2.92
5	0.260	0.120	0.320	81.15	15.58	3.27
6	0.400	0.160	0.480	86.62	11.16	2.22
7	0.580	0.200	0.680	78.73	18.06	3.21
8	0.800	0.240	0.920	88.12	8.98	2.90
9	1.060	0.280	1.200	95.00	3.00	2.00
10	1.360	0.320	1.520			
11	1.700	0.360	1.880	92.50	4.00	3.50
12	2.080	0.400	2.280			
13	2.500	0.440	2.720	90.00	5.00	5.00
14	2.990	0.540	3.260			
15	3.580	0.640	3.900			
16	4.270	0.740	4.640	68.00	20.00	12.00
17	5.060	0.840	5.480			

18	5.950	0.940	6.420			
19	6.940	1.040	7.460			
20	7.980	1.040	8.500			

Layer node depth (Z_i), thickness (ΔZ_i), and depth at layer interface ($Z_{h,i}$) for default soil column. All in meters.

Accordingly, we revised the sentences in lines 174-186 as "The soil hydraulic parameters, including the porosity, saturated hydraulic conductivity, hydraulic potential, the Clapp-Hornberger parameter b, field capacity, wilt point, and saturated soil water diffusivity, were determined using the pedotransfer functions proposed by Hillel (1980), Cosby et al. (1984), and Wetzel and Chang (1987) (Equations S1-S7), in which the sand and clay percentages were based on Hu et al., (2017) (Table S1). In addition, the simulation depth was extended to 8.0 m to cover the active layer thickness of the QTP. The soil column was discretized into 20 layers, whose depths follow the default scheme in CLM 5.0 (Table S1, Lawrence et al., 2018). Due to the inexact match between observed and simulated depths, the simulations at 4cm, 26cm, 80cm, 136cm, 208cm and 299cm were compared with the observations at 5cm, 25cm, 70cm, 140cm, 220cm and 300cm, respectively. A 30-year spin-up was conducted in every simulation to reach equilibrium soil states.".

List of changes

Please note that all the lines in our responses refer to the line numbers in the marked-up manuscript, which shows all the changes and is appended at the end of this response.

1. We have rerun the simulations involving RUN(3) as replied to the comment #3 from referee #2, and all the figures in the manuscript have been revised accordingly.

2. Analyses and discussions for impacts of snow-related processes on soil temperature in Sec. 3.1.1 and Sec. 4.1, respectively.

3. Evaluation and discussions on the performance of Noah-MP on soil liquid water (SLW) have been added in lines 280-287, lines 322-327, lines366-393, and Sec. 4.3.3.

4. Results are analyzed for frozen (October-April) and thawed (May-September) soil conditions separately in Sec. 3.2.1 and Sec. 3.2.2.

5. Detailed information on soil discretization scheme, soil particle fraction, and pedotransfer functions have been added in the supplementary file.

6. More detailed description about the study site in lines 126-131, and limitations and outlooks of this study in lines 603-612.

7. Thanks to the funded projects and referees in lines 683-688.

8. All the unfrozen water in the manuscript have been revised as soil liquid water (SLW).

9. Delete "under review" in line 161.

10. Rewrite the sentences in lines 193-196.

11. The study of Li et al. (2015) is cited in line 200:

    Li, K., Gao, Y., Fei, C., Xu, J., Jiang, Y., Xiao, L., Li, R., and Pan, Y.: Simulation of impact of roots on soil moisture and surface fluxes over central Qinghai − Xizang Plateau. Plateau Meteor., 34, 642-652, https://doi.org/10.7522/j.issn.1000-0534.2015.00035, 2015.

12. Delete the interaction analysis part in lines 328-346.

13. All typos have been corrected.

1 **Assessing the simulated soil thermal regime from Noah-MP LSM**

2 **v1.1 for near-surface permafrost modeling on the Qinghai-Tibet**

3 **Plateau**

4

5 Xiangfei Li[1,2], Tonghua Wu[1,*], Xiaodong Wu[1], Xiaofan Zhu[1], Guojie Hu[1], Ren Li[1],

6 Yongping Qiao[1], Cheng Yang[1,2], Junming Hao[1,2], Jie Ni[1,2], Wensi Ma[1,2]

7

8 [1] Cryosphere Research Station on the Qinghai-Tibet Plateau, State Key Laboratory of

9 Cryospheric Science, Northwest Institute of Eco-Environment and Resources, Chinese

10 Academy of Sciences, Lanzhou 730000, China

11 [2] University of Chinese Academy of Sciences, Beijing 100049, China

12

13 **Correspondence:** Tonghua Wu (thuawu@lzb.ac.cn)

14

Abstract. Land surface models (LSMs) are effective tools for near-surface permafrost modeling. Extensive and rigorous model inter-comparison is of great importance before application due to the uncertainties in current LSMs. This study designed an ensemble of 6912 experiments to evaluate the Noah land surface model with multi-parameterization (Noah-MP) for soil temperature (ST) and soil liquid water (SLW) simulation, and investigate the sensitivity of parameterization schemes at a typical permafrost site on the Qinghai-Tibet Plateau. The results showed that Noah-MP systematically overestimates snow cover and thus induces great cold bias in ST. After removing the snow process, Noah-MP generally underestimates STthe cold bias remain, especially that during the cold season. In addition,And the simulation uncertainty of ST is greater in the cold season (October-April) and for the deep soil layers. ST is most sensitive to surface layer drag coefficient (SFC) while largely influenced by runoff and groundwater (RUN). By contrast, the influence of canopy stomatal resistance (CRS) and soil moisture factor for stomatal resistance (BTR) on ST is negligible. With limited impacts on ST simulation, vegetation model (VEG), canopy gap for radiation transfer (RAD) and snow/soil temperature time scheme (STC) are more influential on shallow ST, while super-cooled liquid water (FRZ), frozen soil permeability (INF) and lower boundary of soil temperature (TBOT) have greater impacts on deep ST. In addition, Noah-MP generally underestimates soil moisture. The RUN process dominates the SLW simulation in comparison of the very limited impacts of all other physical processes. Furthermore, an optimal configuration of Noah-MP for permafrost modeling were extracted based on the connectivity between schemes, and they are: table leaf area index with calculated vegetation fraction, Jarvis scheme for CRS, Noah scheme for BTR, BATS model for RUN, Chen97 for SFC, zero canopy gap for RAD, variant freezing-point depression for FRZ, hydraulic parameters defined by soil moisture for INF, ST at 8 m for TBOT, and semi-implicit method for STC. The analysis of the model structural uncertainties and characteristics of each scheme would be constructive to a better understanding of the land surface processes on the QTP and further model improvements towards near-surface permafrost modeling using the LSMs.

1 Introduction

The Qinghai-Tibet Plateau (QTP) hosts the world's largest high-altitude permafrost covering a contemporary area of 1.06×10^6 km^2 (Zou et al., 2017). Under the background of climate warming and intensifying human activities, permafrost on the QTP has been widely suffering thermal degradation (Ran et al., 2018), resulting in reduction of permafrost extent, disappearing of permafrost patches and thickening of active layer (Chen et al., 2020). Moreover, such degradation could cause alterations in hydrological cycles (Zhao et al., 2019; Woo, 2012), changes on ecosystem (Fountain et al., 2012; Yi et al., 2011) and damages to infrastructures (Hjort et al., 2018). Therefore, it is very important to monitor and simulate the state of permafrost to adapt to the degradation.

Soil temperature (ST) is an intuitive indicator to evaluate the thermal state of permafrost. A number of monitoring sites have been established on the QTP (Cao et al., 2019). However, it is inadequate to construct the thermal state of permafrost by considering the spatial variability of the ground thermal regime and an uneven distribution of these observations. In contrast, numerical models are competent alternatives. In recent years, land surface models (LSMs), which describe the exchanges of heat, water, and momentum between the land and atmosphere (Maheu et al., 2018), have received significant improvements in the representation of permafrost and frozen ground processes (Koven et al., 2013; Nicolsky et al., 2007; Melton et al., 2019). LSMs are capable of simulating the transient change of permafrost by describing subsurface hydrothermal processes (e.g. soil temperature and moisture) with soil heat conduction (-diffusion) and water movement equations (Daniel et al., 2008). Moreover, they can be integrated with the numerical weather prediction system like WRF (Weather Research and Forecasting), making them as effective tools for comprehensive interactions between climate and permafrost (Nicolsky et al., 2007).

Some LSMs have been applied to modeling permafrost in the QTP. Guo and Wang (2013) investigated near-surface permafrost and seasonally frozen ground states as well as their changes using the Community Land Model, version 4 (CLM4). Hu et al. (2015)

applied the coupled heat and mass transfer model to identify the hydrothermal characteristics of the permafrost active layer in the Qinghai-Tibet Plateau. Using an augmented Noah LSM, Wu et al. (2018) modeled the extent of permafrost, active layer thickness, mean annual ground temperature, depth of zero annual amplitude and ground ice content on the QTP in 2010s. Despite those achievements based on different models, LSMs are in many aspects insufficient for permafrost modeling. For one thing, large uncertainties still exist in the state-of-the-art LSMs when simulating the soil hydrothermal regime on the QTP (Chen et al., 2019). For instance, 19 LSMs in CMIP5 overestimate snow depth over the QTP (Wei and Dong, 2015), which could result in the variations of the soil thermal regime in the aspects of magnitude and vector (cooling or warming) (Zhang, 2005). Moreover, most of the existing LSMs are not originally developed for permafrost modeling. Many of their soil processes are designed for shallow soil layers (Westermann et al., 2016), but permafrost may occur in the deep soil. And the soil column is often considered homogeneous, which can not represent the stratified soil common on the QTP (Yang et al., 2005). Given the numerous LSMs and possible deficiencies, it is necessary to assess the parameterization schemes for permafrost modeling on the QTP, which is helpful to identify the influential sub-processes, enhance our understanding of model behavior, and guide the improvement of model physics (Zhang et al., 2016).

Noah land surface model with multi-parameterization (Noah-MP) provides a unified framework in which a given physical process can be interpreted using multiple optional parameterization schemes (Niu et al., 2011). Due to the simplicity in selecting alternative schemes within one modeling framework, it has been attracting increasing attention in inter-comparison work among multiple parameterizations at point and watershed scales (Hong et al., 2014; Zheng et al., 2017; Gan et al., 2019; Zheng et al., 2019; Chang et al., 2020; You et al., 2020). For example, Gan et al. (2019) carried an ensemble of 288 simulations from multi-parameterization schemes of six physical processes, assessed the uncertainties of parameterizations in Noah-MP, and further revealed the best-performing schemes for latent heat, sensible heat and terrestrial water

4

storage simulation over ten watersheds in China. You et al. (2020) assessed the performance of Noah-MP in simulating snow process at eight sites over distinct snow climates and identified the shared and specific sensitive parameterizations at all sites, finding that sensitive parameterizations contribute most of the uncertainties in the multi-parameterization ensemble simulations. Nevertheless, there is little research on the inter-comparison of soil thermal processes toward permafrost modeling. In this study, an ensemble experiment of totally 6912 scheme combinations was conducted at a typical permafrost monitoring site on the QTP. The simulated soil temperature (ST) of Noah-MP model was assessed and the sensitivities of parameterization schemes at different depths were further investigated. Considering the general performance and sensitive schemes of Noah-MP, we further explored the interactions between the most influential schemes and configured an optimal combination based on the connections between schemes. We hope this study can provide a reference for permafrost simulation on the QTP.

This article is structured as follows: Section 2 introduces the study site, atmospheric forcing data, design of ensemble simulation experiments, and sensitivity analysis and optimal selection methods. Section 3 describes the ensemble simulation results of ST, explores the sensitivity and interactions of parameterization schemes, and determines the optimal combination for permafrost modeling. Section 4 discusses the schemes in each physical process and proposes further research topics. Section 5 concludes the main findings of this study.

2 Methods and materials

2.1 Site description and observation datasets

Tanggula observation station (TGL) lies in the continuous permafrost regions of Tanggula Mountain, central QTP (33.07°N, 91.93°E, Alt.: 5,100 m a.s.l; Fig. 1). This site a typical permafrost site on the plateau with sub-frigid and semiarid climate (Li et al., 2019), filmy and discontinuous snow cover (Che et al., 2019), sparse grassland (Yao

5

et al., 2011), coarse soil (Wu and Nan, 2016; He et al., 2019), and thick active layer (Luo et al., 2016), which are common features in the permafrost regions of the plateau. is characterized by the sub-frigid and semiarid climate (Li et al., 2019). According to the observations from 2010−2011, the annual mean air temperature of TGL site was −4.4 °C. The annual precipitation was 375 mm, and of which 80% is concentrated between May and September. Alpine steppe with low height is the main land surface, whose coverage range is about 40% ~ 50% (Yao et al., 2011). The active layer thickness is about 3.15 m (Hu et al., 2017).

The atmospheric forcing data, including wind speed/direction, air temperature/relative humidity/pressure, downward shortwave/longwave radiation, and precipitation, were used to drive the model. These variables above were measured at a height of 2 m and covered the period from August 10, 2010 to August 10, 2012 (Beijing time) with a temporal resolution of 1 hour. Daily soil temperature and liquid moisture at depths of 5cm, 25cm, 70cm, 140cm, 220cm and 300cm from October 1, 2010 to September 30, 2011 (Beijing time) were utilized to validate the simulation results.
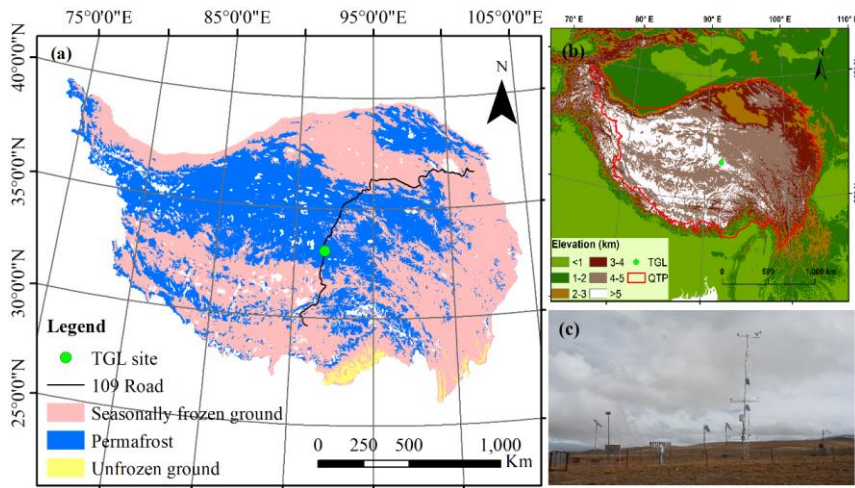
Figure 1. Location and geographic features of study site. (a) Location of observation site and permafrost distribution (Zou et al., 2017). (b) Topography of the Qinghai-Tibet Plateau. (c) Photo of the Tanggula observation station.

2.2 Ensemble experiments of Noah-MP

The offline Noah-MP LSM v1.1 was assessed in this study. It consists of 12 physical processes that are interpreted by multiple optional parameterization schemes. These sub-processes include vegetation model (VEG), canopy stomatal resistance (CRS), soil moisture factor for stomatal resistance (BTR), runoff and groundwater (RUN), surface layer drag coefficient (SFC), super-cooled liquid water (FRZ), frozen soil permeability (INF), canopy gap for radiation transfer (RAD), snow surface albedo (ALB), precipitation partition (SNF), lower boundary of soil temperature (TBOT) and snow/soil temperature time scheme (STC) (Table 1). Details about the processes and optional parameterizations can be found in Yang et al. (2011a).

In this study, the dynamic vegetation option in VEG process was turned off for simplicity. Previous studies has confirmed that Noah-MP seriously overestimate the snow depth on the QTP (Li et al., 2020 (under review); Wang et al., 2020). However, the impact of snow cover on ground temperatures in the permafrost regions of QTP is usually considered weak (Jin et al., 2008; Wu et al., 2018), because the snow cover is thin, short-lived, and patchy-distributed (Che et al., 2019). For practical purpose To avoid the possible bias caused by snow process, the ALB and SNF processes were not considered by setting the snow fraction in precipitation to zero. Since no snow cover in the ground, the ground albedo equals the soil albedo. As a result, in total 6912 combinations are possible for the left 10 processes and orthogonal experiments were carried out to evaluate their performance in soil thermal dynamics and obtain the optimal combination.

The monthly leaf area index (LAI) was derived from the Advanced Very High-Resolution Radiometer (AVHRR) (https://www.ncei.noaa.gov/data/, Claverie et al., 2016). The Noah-MP model was modified to consider the vertical heterogeneity in the soil profile by setting the corresponding soil parameters for each layer. The soil hydraulic parameters, including the porosity, saturated hydraulic conductivity, hydraulic potential, the Clapp-Hornberger parameter b, field capacity, wilt point, and saturated soil water diffusivity, were determined using the pedotransfer functions

7

proposed by Hillel (1980), Cosby et al. (1984), and Wetzel and Chang (1987) (Equations S1-S7), in which the sand and clay percentages were based on Hu et al., (2017) (Table S1). In addition, the simulation depth was extended to 8.0 m to cover the active layer thickness of the QTP. The soil column was discretized into 20 layers, whose depths following the default scheme in CLM 5.0 (Table S1, Lawrence et al., 2018). Due to the inexact match between observed and simulated depths, the simulations at 4cm, 26cm, 80cm, 136cm, 208cm and 299cm were compared with the observations at 5cm, 25cm, 70cm, 140cm, 220cm and 300cm, respectively. A 30-year spin-up was conducted in every simulation to reach equilibrium soil states.

Table 1. The physical processes and options of Noah-MP. Options in bold are the optimal selections in this study.

Physical processes	Options
Vegetation model (VEG)	(1) table LAI, prescribed vegetation fraction
	(2) dynamic vegetation
	(3) table LAI, calculated vegetation fraction
	(4) table LAI, prescribed max vegetation fraction
Canopy stomatal resistance (CRS)	**(1) Jarvis**
	(2) Ball-Berry
Soil moisture factor for stomatal resistance (BTR)	**(1) Noah**
	(2) CLM
	(3) SSiB
Runoff and groundwater (RUN)	(1) SIMGM with groundwater
	(2) SIMTOP with equilibrium water table
	(3) Noah (free drainage)
	(4) BATS (free drainage)
Surface layer drag coefficient (SFC)	(1) Monin-Obukhov (M-O)
	(2) Chen97
Super-cooled liquid water (FRZ)	(1) generalized freezing-point depression
	(2) Variant freezing-point depression
Frozen soil permeability (INF)	**(1) Defined by soil moisture, more permeable**
	(2) Defined by liquid water, less permeable
Canopy gap for radiation transfer (RAD)	(1) Gap=F(3D structure, solar zenith angle)
	(2) Gap=zero
	(3) Gap=1-vegetated fraction
Snow surface albedo (ALB)	(1) BATS
	(2) CLASS
Precipitation partition (SNF)	(1) Jordan91
	(2) BATS: $T_{sfc} < T_{frz}+2.2K$
	(3) $T_{sfc} < T_{frz}$

8

Lower boundary of soil temperature (TBOT)	(1) zero heat flux **(2) soil temperature at 8m depth**
Snow/soil temperature time scheme (STC)	**(1) semi-implicit** (2) full implicit

189 BATS (Biosphere–Atmosphere Transfer Model); CLASS (Canadian Land Surface Scheme);

190 SIMGM (Simple topography-based runoff and Groundwater Model); SIMTOP (Simple

191 Topography-based hydrological model); SSiB (Simplified Simple Biosphere model).

2.3 Methods for sensitivity analysis

192

193 The root mean square error (RMSE) ~~and standard deviation (SD)~~ between the

194 simulations and observations were adopted to evaluate the performance of Noah-MP.

195 The averages of the RMSEs ~~and SDs~~ of all the soil layers were defined as column

196 RMSE (colRMSE) ~~and column SD (colRMSE), respectively~~.

197 To investigate the influence degrees of each physical process on ST and SLW, we

198 firstly calculated the mean RMSE ($\bar{Y}_j^i$) of the jth parameterization schemes ($j = 1, 2, \ldots$)

199 in the ith process ($i = 1, 2, \ldots$). Then, the maximum difference of $\bar{Y}_j^i$ ($\Delta\overline{RMSE}$) was

200 defined to quantify the sensitivity of the ith process ($i = 1, 2, \ldots$) (Li et al., 2015):

201
$$\Delta\overline{RMSE} = \bar{Y}_{max}^i - \bar{Y}_{min}^i$$

202 where $\bar{Y}_{max}^i$ and $\bar{Y}_{min}^i$ are the largest and the smallest $\bar{Y}_j^i$ in the ith process,

203 respectively. For a given physical process, a high $\Delta\overline{RMSE}$~~s~~ signifies large difference

204 between parameterizations, indicating high sensitiveness of the ith process.

205 The sensitivities of physical processes were determined by quantifying the

206 statistical distinction level of performance between parameterization schemes. The

207 Independent-sample T-test (2-tailed) was adopted to identify whether the distinction

208 level between two schemes is significant, and that between three or more schemes was

209 tested using the Tukey's test. Tukey's test has been widely used for its simple

210 computation and statistical features (Benjamini, 2010). The detailed descriptions about

211 this method can be found in Zhang et al. (2016), Gan et al. (2019), and You et al. (2020).

212 A process can be considered sensitive when the schemes show significant difference.

213 Moreover, schemes with small mean RMSE were considered favorable for ST/SLW

214 simulation. We distinguished the differences of the parameterization schemes at 95%

215 confidence level.

216 **2.4 Optimal selection methods**

217 To extract the optimal combinations of parameterization schemes, the connection

218 frequency (CF) between parameterizations was calculated:

219 (1) Sorting the 6912 colRMSEs in an ascending order;

220 (2) Donating the colRMSEs concentrated below the 5th percentile as the "best

221 combinations" (346 members);

222 (3) Counting the times of a given parameterizations occurring with other

223 parameterizations in the "best combinations";

224 (4) The CF was then determined by dividing 346.

225 Obviously, for two given parameterization schemes, a large CF has an advantage

226 in terms of optimal combination.

227 **3   Results**

228 **3.1 General performance of the ensemble simulation**

229 **3.1.1 Snow process simulation**

230 The performance of Noah-MP for snow simulation and its impacts on soil

231 temperature was firstly tested by conducting an ensemble of 41472 (= 6912*2*3)

232 experiments. Due to a lack of snow depth measurements, ground albedo was used as an

233 indicator for snow cover. Figure 1 shows the monthly variations of observed ground

234 albedo and the simulations produced by the ensemble simulations considering snow-

235 related physical processes (i.e. the ALB and SNF processes). The ground albedo was

236 extremely overpredicted with large uncertainties when considering the snow options in

237 Noah-MP, indicating the overestimation of snow depth and duration. As a result, the

10

soil temperature basically presented a huge cold bias and large uncertainties at all layers (Fig. S1). When neglecting the snow, the simulated ground albedo was nearer to the observation with a mean absolute error of 0.06. And the underestimation and uncertainties of soil temperature was greatly resolved.

The influence of snow cover on soil temperature was further analyzed based on in-situ measurements. Figure 3 shows the meteorological conditions and soil temperatures during a long-term snow process from 12/28/2010 – 1/27/2011. It can be seen that shallow soil temperature (5cm, 25cm, and 70cm) basically fluctuated with air temperature. At the beginning of the snow events on 1/1/2011, soil temperature at 5cm, 25cm, and 70cm was slightly increased by 1.5℃, 1.2℃, and 0.7 ℃, respectively. With the melting of snow, the amplitude of soil temperature decreased. Meanwhile, soil temperature at deep layers showed no obvious fluctuations during the whole period. It indicates that snow cover at TGL site has a very limited effect on soil temperature, especially that of deep layers.

Given the poor simulation of Noah-MP for snow cover and the weak impact of snow on soil temperature in reality, we will focus on the results of ensemble simulations without considering snowfall (6912 experiments in total) in the following sections.
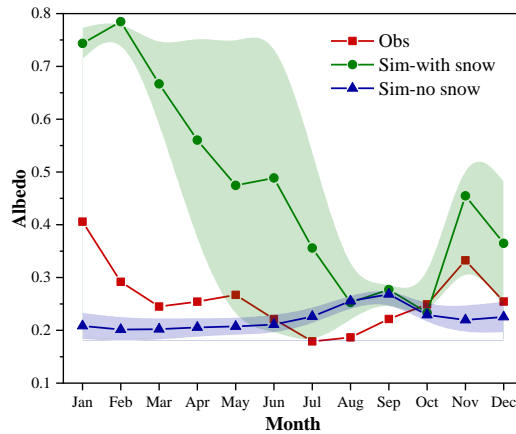
Figure 2. Monthly variations ground albedo at TGL site for observation (Obs), the ensemble simulation considering snow (Sim-with snow), and ensemble simulation neglecting snow (Sim-no snow). The green shadow represents the standard deviation

259 of the ensemble simulation.

260
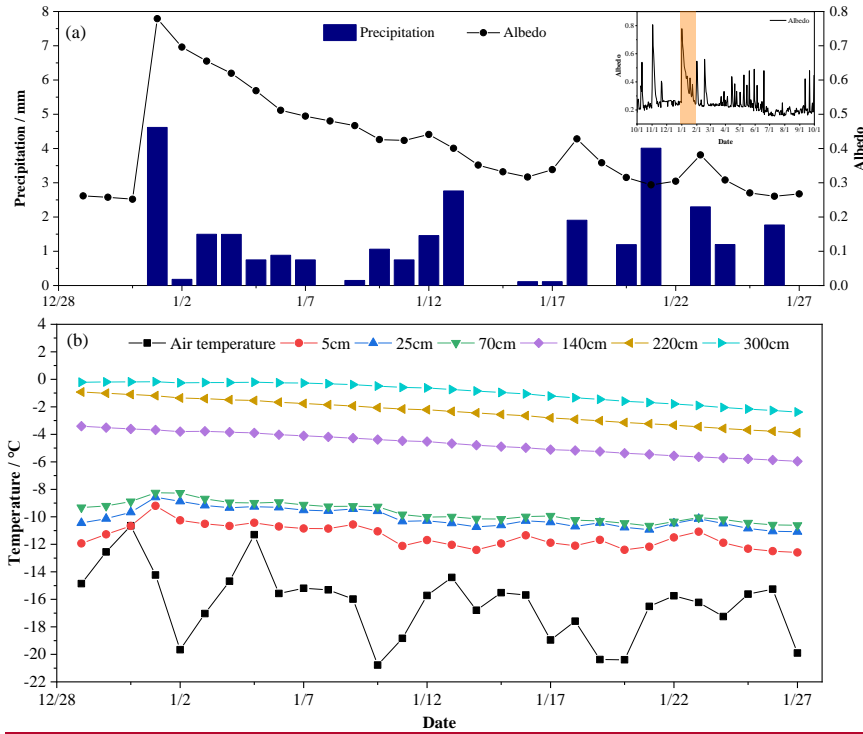
262 **Figure 3.** Variations of (a) precipitation and ground albedo, (b) air temperature and soil
263 temperature at TGL site from 28 December 2010 to 27 January 2011.

264 **3.1.2 Soil temperature and moisture simulation**

265 　　We evaluated ST from the 6912 experiments against observations. Figure. ~~2~~ 4
266 illustrates the ensemble simulated and observed annual cycle of ST at TGL site. The
267 plots give the uncertainty ranges of the ensemble experiments using five statistical
268 indicators, i.e., the first/third quartile (Q1/Q3), mean, the lower (Q1-1.5(Q3-Q1)) and
269 upper bound (Q3+1.5(Q3-Q1)). The kernel density distribution of the simulated ST is
270 also illustrated. The ensemble experiments basically captured the seasonal variability
271 of ST, whose magnitude decreased with soil depth. In addition, the simulated ST in the
272 cold season (October-April) showed relatively wide uncertainty ranges, particularly at
273 the deep layers. This indicates that the selected schemes perform more differently

12

during the cold season, which is especially so at the deep layers. The simulated ST were generally smaller than the observations with relatively large gap during the cold season. It indicates that the Noah-MP model generally underestimates the ST, especially during the cold season. Moreover, the simulated ST was widely found to be bimodal distribution across the soil column, implying that two schemes dominate the ST simulation in the Noah-MP model.

Since the observation equipment can only record the liquid water, soil liquid water (SLW) was evaluated against simulations from the 6912 experiments (Fig. 5). The Noah-MP model generally underestimated surface (5cm and 25cm) and deep (300cm) SLW (Fig. 5g, 5h, 5l). However, Noah-MP tended to overestimate the SLW at the middle layers of 70cm, 140cm and 220cm. Moreover, the simulated SLW exhibited relatively wide uncertainty ranges during the warm season, particularly at the middle layers (Fig. 5). In addition, the distribution of the simulated SLW showed distinct bimodal peaks at the depth of 70cm and 140cm.
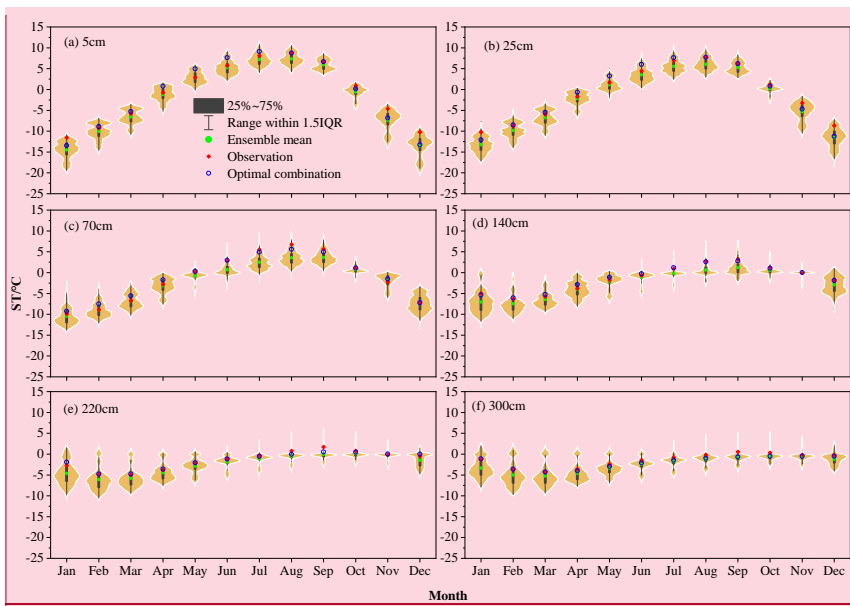
批注 [LX1]: deleted
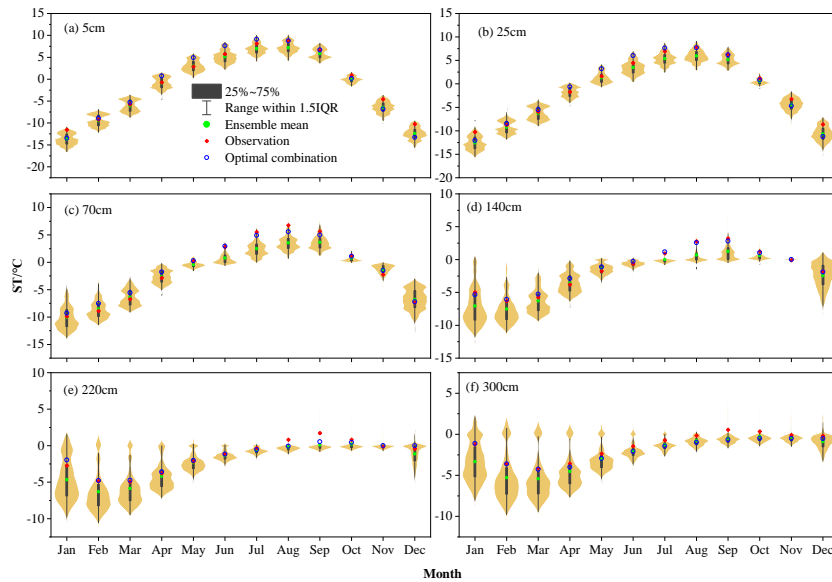
Figure 2̶4. Monthly soil temperature (ST) at (a) 5 cm, (b) 25 cm, (c) 70 cm, (d) 140 cm, (e) 220 cm, (f) 300 cm at TGL site. Limits of the boxes represent upper and lower quartiles, whiskers extend to 1.5 times the interquartile range (IQR). The green circles in the box are the ensemble mean values. The light orange shading represents the kernel density distribution of simulated ST. The red diamonds are observations and the blue circles are the results of the optimal scheme combination.

14
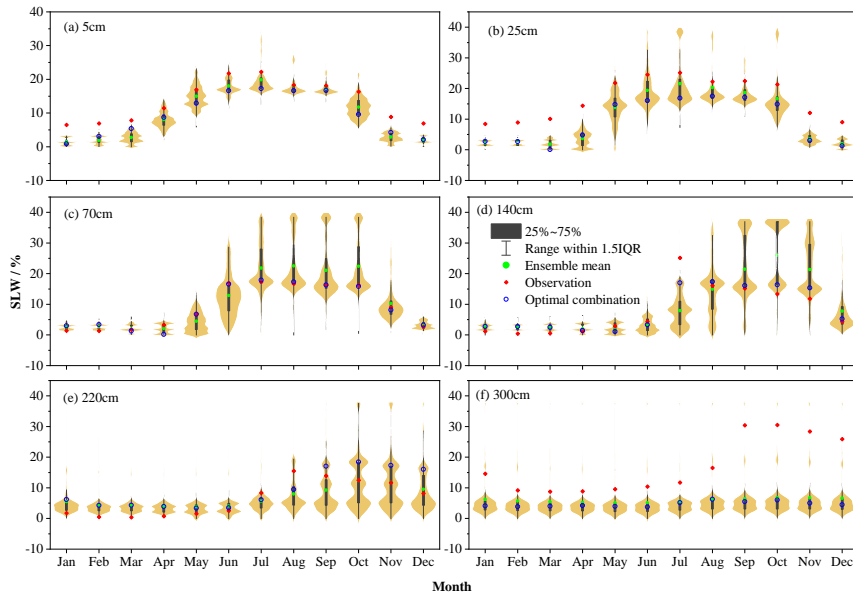
Figure 5. Same as in Figure 4 but for SLW.

3.2 Sensitivity of physical processes

3.2.1 Influence degrees of physical processes

批注 [LX2]: deleted

15
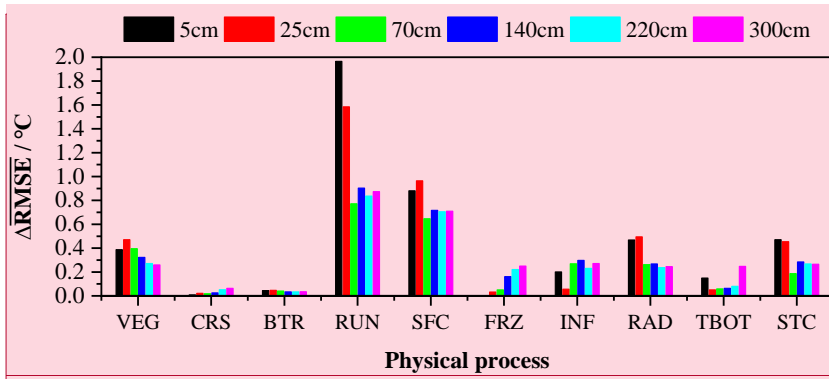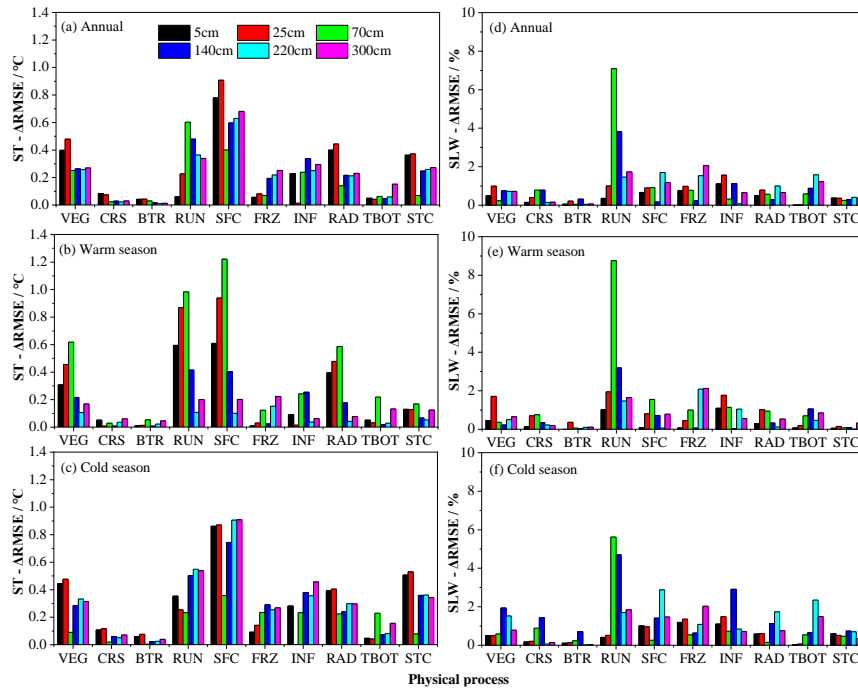
Figure 3~~3~~6. The maximum difference of the mean RMSE ~~(ΔRMSE)~~ for (a, b and c) soil temperature (ST-Δ$\overline{RMSE}$ in °C) and (d, e and f) soil liquid water (SLW-Δ$\overline{RMSE}$ in %) in each physical process during the (a and d) annual, (b and e) warm season, and (c and f) cold season at different soil depths.

Figure. ~~3~~6 compares the influence scores of the 10 physical processes at different soil depths, based on the maximum difference of the mean RMSE over 6912 experiments using the same scheme, for ST and SLW at TGL site. The SFC and RUN ~~and SFC~~ processes dominated the ST-Δ$\overline{RMSE}$ at all layers, indicating that they are the most sensitive processes for ST simulation. While most of the ST-Δ$\overline{RMSE}$ of the other 8 physical processes were ~~all~~ less than 0.~~5~~6°C, among which the influence of CRS and BTR processes were negligible. What's more, the VEG, RAD and STC processes were more influential on the shallow STs than the deep STs. Taking the ~~STC~~ RAD process as an example, the annual ST-Δ$\overline{RMSE}$ of the 5cm and 25 cm were nearly 0.~~5~~4°C while that of the 70 cm, 140cm, 220cm and 300cm were ~~no more than~~around 0.~~3~~2°C. In contrast, the influence of FRZ, INF and TBOT processes were generally greater in deep

16

soils than shallow soils. During the warm season, the physical processes generally showed more influence on shallow soil temperatures. When it comes to the cold season, the influence of the physical processes on deep layers obviously increased and comparable with that on shallow layers, implying the relatively higher uncertainties of Noah-MP during the cold season.

Most $\Delta\overline{RMSE}$ for SLW are far less than 10%, indicating that all the physical processes have limited influence on the SLW, among which CRS, BTR, and STC showed the smallest effects on SLW (Fig. 6d). The RUN process dominates the performance of SLW simulation, especially at lower layers (70cm and 140cm, Fig. 6d, 5e, and 5f). In addition, the VEG, SFC, FRZ, RAD, and TBOT processes generally showed more influence on deep layers, particularly in the cold season.

Interactions between two of the most influential physical processes are analyzed in this section. The performance of the simulations with SFC and RUN were rated by rounding the colRMSEs and colSDs (Fig. 4). Given the colRMSE=1.2 for one simulation, then the score of the simulation equals 1 (SCORE=1) for the corresponding combination. It can be seen that SFC(1) in the SFC process and RUN(3) in the RUN process were the major schemes that contribute to the cold bias of the ensemble simulation, because they dominated the cold bias of the ensemble simulation with relatively low colSD scores (Fig. 4b). Consistent with the bimodal distribution in Fig. 2, most of the simulations with relative low colRMSE and nearly zero colSD were related to SFC(2). It indicates that combinations with SFC(2) result in better performance than SFC(1) by improving the underestimations of ST. Among the schemes in RUN, RUN(1), RUN(2) and RUN(4) had approximately equal chance to produce better and worse performance for ST simulation, implying a dominating role of the SFC process (Fig. 4a). RUN(3) produced much worse performance by aggravating the underestimation of ST. Ultimately, the best results came from the combination of SFC(2) and RUN(4), while the worst results were from the combination of SFC(1) and RUN(3).
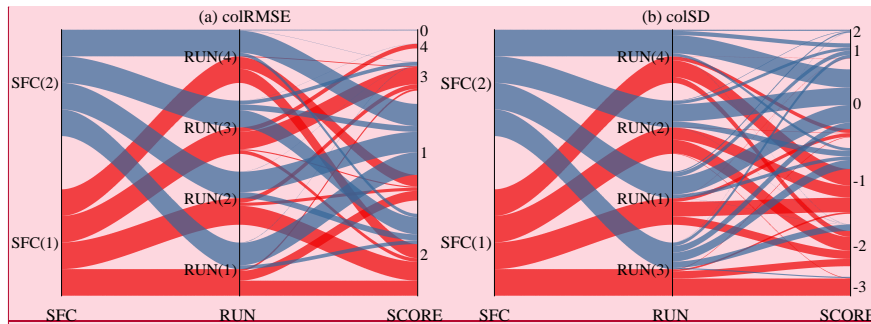
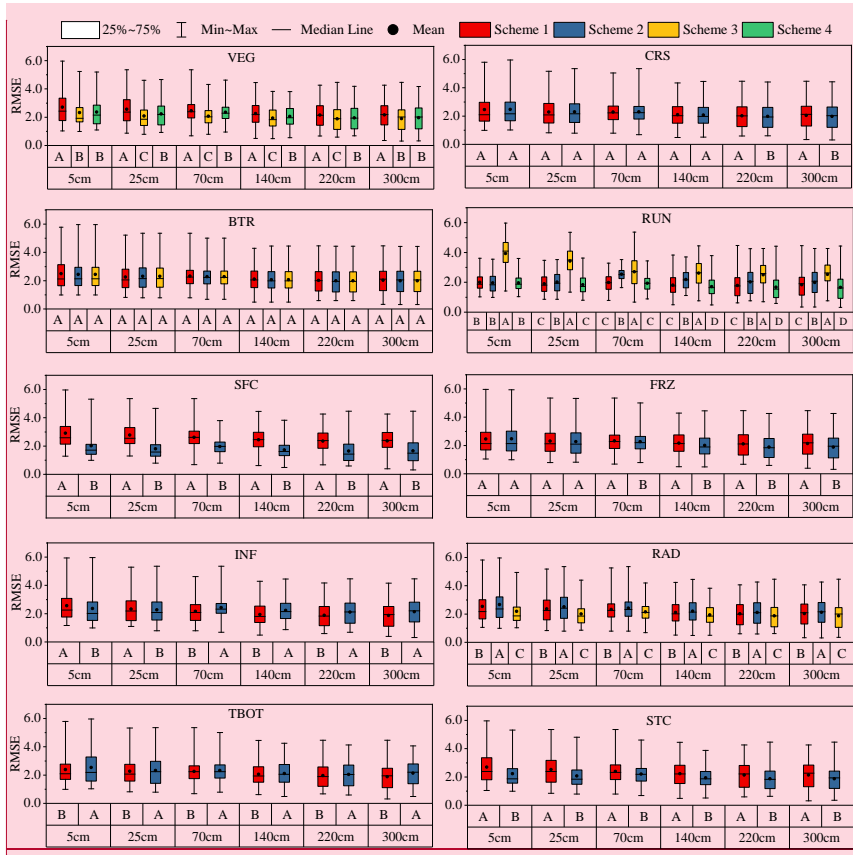**Figure 4.** Rating of combinations with SFC and RUN.

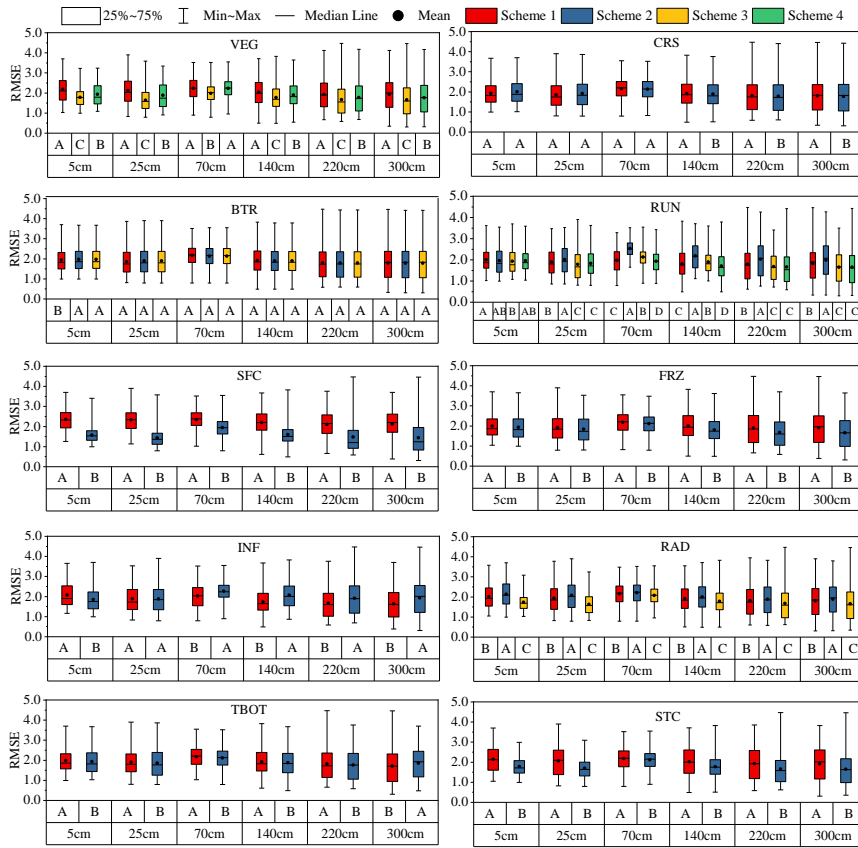### 3.2.2 Sensitivities of physical processes and general behaviors of

parameterizations

To further investigate the sensitivity of each process and the general performance of the parameterizations, the Independent-sample T-test (2-tailed) and Tukey's test were conducted to test whether the difference between parameterizations within a physical process is significant (Fig. 5-7). In a given sub-process, any two schemes labelled with different letters behave significantly different, and this sub-process therefore can be identified as sensitive. Otherwise, the sub-process is considered insensitive. Moreover, schemes with the letters late in the alphabet have smaller mean RMSEs and outperform the ones with the letters forward in the alphabet. Using the three schemes in vegetation model process (hereafter VEG(1), VEG(3) and VEG(4)) in Fig. 5-7 as an example. At the depth of 5cm 70cmand 300cm, VEG(13) was labeled with letter "AB", while VEG(31) and VEG (4) was labeled with letter "BA". For other layers,the depth of 25cm, 70cm, 140cm and 220cm, VEG(1), VEG(3) and VEG(4) were labeled with the letter "A", "C" and "B", respectively. As described above, the VEG process was sensitive for ST simulation. Moreover, VEG(3) and VEG(4) had advantages in producing good simulations than VEG(1) and VEG(4) at 5cm 70cm and 300cm depths, and the performance decreased in the order of VEG(3) > VEG(4) > VEG(1) at other layers. In terms of the whole soil column, VEG(3) outperformed VEG(1) and VEG(4).

Consistent with the result in Fig. 36, all other physical processes showed sensitivities in varying magnitudes except the BTR and CRS process. And the

18

368　performance difference between schemes of the RUN and SFC were obviously greater

369　than other processes. For the RUN process, the performance orders for both ST and

370　SLW simulation generally followed RUN(4) > RUN(1) > RUN(2̶3) > RUN(3̶2) as a

371　whole. For the whole year, RUN(1), RUN(3), and RUN(4) had significant but slightly

372　difference between each other, among which RUN(1) and RUN(4) presented similar

373　performance during both warm and cold seasons (Fig. S2, S3, S4 and S5). During the

374　warm season, the performance of RUN(3) for ST simulation showed notable

375　improvements at shallow layers (5cm and 25cm, Fig. S2). By contrast, RUN(2)

376　performed the worst among the four schemes in spite of the good performance at

377　shallow layers during the cold season (5cm and 25cm in Fig. S3, 25cm in Fig. S5).

378　M̶e̶a̶n̶w̶h̶i̶l̶e̶,̶ ̶t̶h̶e̶ ̶d̶i̶f̶f̶e̶r̶e̶n̶c̶e̶ ̶b̶e̶t̶w̶e̶e̶n̶ ̶R̶U̶N̶(̶1̶)̶ ̶a̶n̶d̶ ̶R̶U̶N̶(̶4̶)̶ ̶w̶a̶s̶ ̶i̶n̶d̶i̶s̶t̶i̶n̶c̶t̶i̶v̶e̶ ̶a̶t̶ ̶t̶h̶e̶

379　s̶h̶a̶l̶l̶o̶w̶ ̶l̶a̶y̶e̶r̶s̶ ̶(̶5̶ ̶c̶m̶,̶ ̶2̶5̶ ̶c̶m̶ ̶a̶n̶d̶ ̶7̶0̶ ̶c̶m̶)̶ ̶a̶n̶d̶ ̶s̶i̶g̶n̶i̶f̶i̶c̶a̶n̶t̶ ̶b̶u̶t̶ ̶v̶e̶r̶y̶ ̶s̶m̶a̶l̶l̶ ̶a̶t̶ ̶t̶h̶e̶ ̶d̶e̶e̶p̶ ̶l̶a̶y̶e̶r̶s̶

380　(̶1̶4̶0̶ ̶c̶m̶,̶ ̶2̶2̶0̶ ̶c̶m̶ ̶a̶n̶d̶ ̶3̶0̶0̶ ̶c̶m̶)̶.̶ During both warm and cold seasons,M̶o̶r̶e̶o̶v̶e̶r̶,̶ the

381　performance orders for ST simulations were SFC(2) > SFC(1) for SFC process, FRZ(2) >

382　FRZ(1) for FRZ process, and RAD(3) > RAD(1) > RAD(2) for RAD process (Fig. S2

383　and S3), T̶B̶O̶T̶(̶1̶)̶ ̶>̶ ̶T̶B̶O̶T̶(̶2̶)̶ ̶f̶o̶r̶ ̶T̶B̶O̶T̶ ̶p̶r̶o̶c̶e̶s̶s̶,̶ ̶a̶n̶d̶ ̶S̶T̶C̶(̶2̶)̶ ̶>̶ ̶S̶T̶C̶(̶1̶)̶ ̶f̶o̶r̶ ̶S̶T̶C̶

384　p̶r̶o̶c̶e̶s̶s̶which are particularly so for SLW simulations at shallow and deep layers. In

385　particular, the FRZ process showed higher sensitivity at the deep soils and during the

386　cold season (Fig. 6, 7 and 8). i̶n̶ ̶s̶p̶i̶t̶e̶ ̶o̶f̶ ̶t̶h̶e̶ ̶s̶h̶a̶l̶l̶o̶w̶ ̶s̶o̶i̶l̶.̶ For the ST simulation,

387　C̶o̶m̶p̶a̶r̶e̶d̶ ̶w̶i̶t̶h̶ ̶I̶N̶F̶(̶1̶)̶,̶ INF(2) performed better at the shallow soils (5cm and 25cm)

388　while did worse at the deep soils compared with INF(1). Despite the slightly good

389　performance of TBOT(2) for ST simulation at the first five layers, TBOT(1) greatly

390　outperformed TBOT(2) at the depth of 300cm. For the STC process, STC(2) greatly

391　excel STC(1) in simulating ST while showed small different with STC(1) when

392　simulating SLW. However, the impact of STC process on SLW increase in line with

393　that on ST during the cold season (Fig. 6).

Figure 57. Distinction level for RMSE of ST at different layers during the whole year in the ensemble simulations. Limits of the boxes represent upper and lower quartiles, whiskers extend to the maximum and minimum RMSE. The black stations in the box are the average values. The lines in the box indicate the median value.
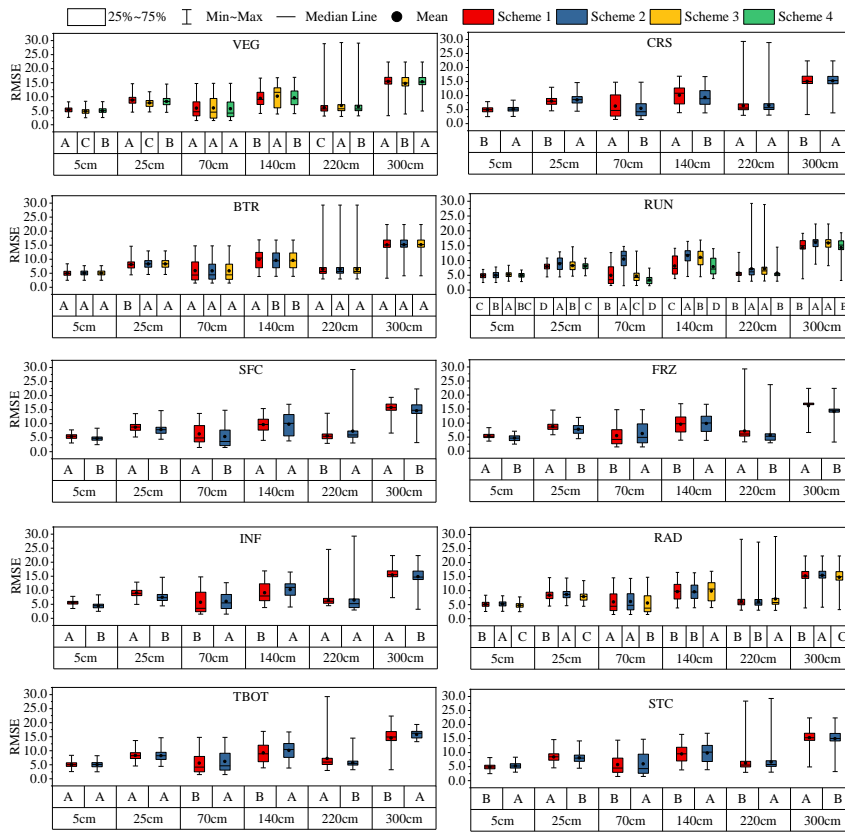
Figure 8. Same as in Figure 7 but for SLW.

3.3 The optimal combination

The CF was calculated to extract the optimal combination of parameterization schemes for ST simulation (Fig. ~~6~~9). The CF between any two schemes from the same physical process was zero as expected. ~~Consistent with Fig. 5, t~~The CF of RUN(2) and RUN(3) with other schemes was nearly zero, implying that using RUN(2) and RUN (3) provides an extreme less chance of producing favorable simulations than using RUN(1)~~, RUN(2) or~~ RUN(4). A higher CF signify greater probability of producing advantageous simulations. For instance, the CF between SFC(2) and VEG(3) was 0.~~45~~46, about two times than the CFs between SFC(2) and VEG(1)/VEG(4). It indicates that ~~45~~46% of the ~~3~~46 best combinations adopted SFC(2) and VEG(3) simultaneously, and the

22

412 combination of SFC(2) and VEG(3) tend to ~~inducing~~ induce better ST in comparison

413 of the combination of SFC(2) and VEG(1)/VEG(4).

414   SFC(2) is firstly determined as one of the schemes that make up the optimal

415 combination, because it was most widely linked to other parameterization schemes with

416 relatively large CFs. Other optimal schemes of each physical process can be determined

417 by choosing the one that has large CF with SFC(2). Obviously, VEG(3), RUN(4),

418 FRZ(2) and INF(1) outperform other schemes in the corresponding physical processes

419 and were selected for optimal combination. The schemes within CRS, BTR, RAD and

420 STC processes scored nearly identical CFs with SFC(2). Due to the insensitivity of CRS

421 and BTR, CRS(1) and BTR(1), which are the default schemes in Noah-MP, were

422 determined as the member schemes of the optimal combination. Combining the selected

423 schemes above with different schemes of RAD and STC processes, there are 6

424 candidate combinations, among which the one with smallest colRMSE is selected as

425 the optimal combination. Ultimately, the determined schemes for optimal combination

426 is VEG(3), CRS(1), BTR(1), RUN(4), SFC(2), FRZ(2), INF(1), RAD(2), TBOT(2) and

427 STC(1) (Table 1).

428   The simulated results of the optimal scheme combination well captured the

429 variation of ST (Fig. 24). Despite the overestimation of ST at the shallow soil layers

430 from April to July, the optimal combination well produced the ST during the cold season

431 and of the deep layers (Fig. 24), which is crucial for modeling permafrost features such

432 as active layer thickness and temperature at the top of the permafrost.

433

434

435
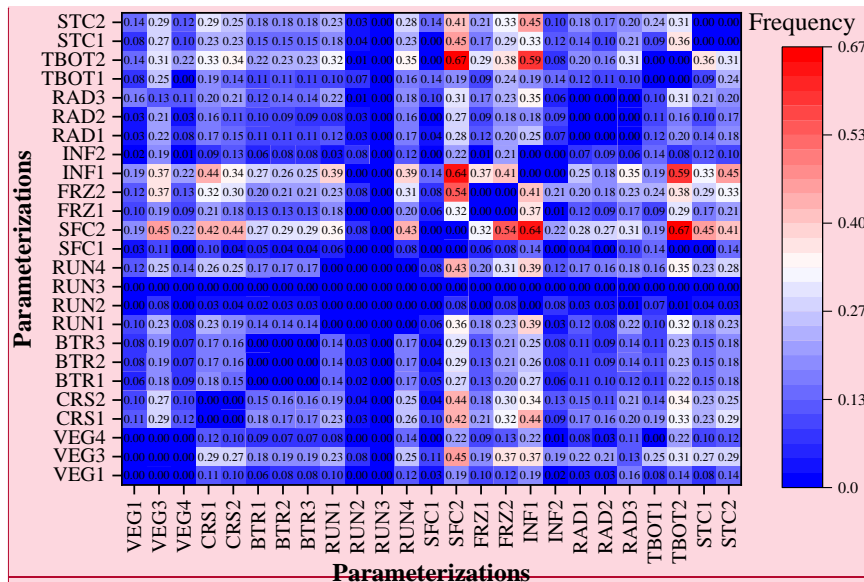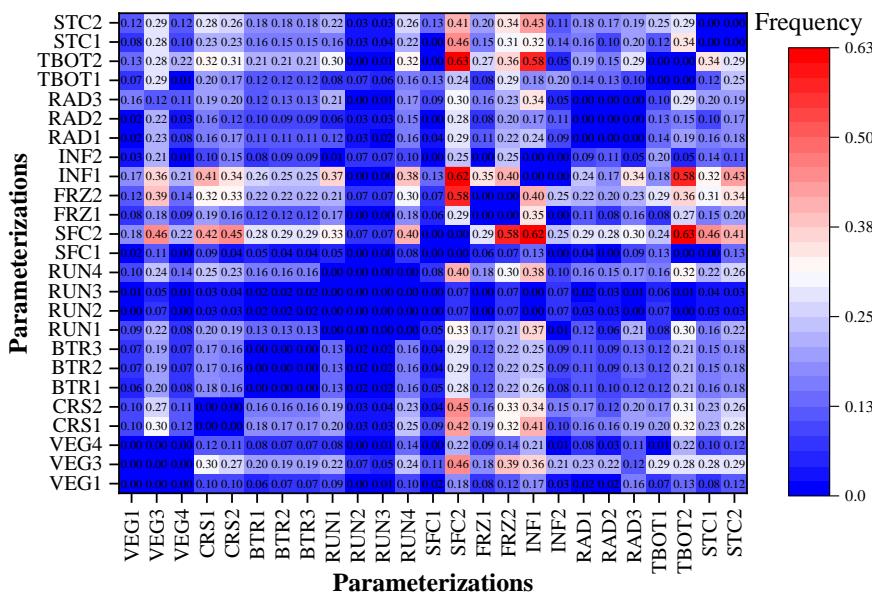
Figure 69. Connection frequency of parameterization schemes.

436

4   Discussion

4.1 Influence of snow cover on permafrost in the QTP

Reproducing the snow processes remains a persistent challenge for LSMs in the QTP, most of which overestimate the snow depth (Wei and Dong, 2015), including the Noah-MP model (Jiang et al., 2020; Li et al., 2020; Wang et al., 2020). Our ensemble simulations also show that the surface albedo is extremely overestimated in both magnitude and duration (Fig. 2), implying an extreme overestimation of snow cover. The overestimation is ascribed to many causes, such as the vegetation effect (Park et al., 2016), the snow cover fraction (Jiang et al., 2020), the sublimation from wind (Yuan et al., 2016; Li et al., 2020), and the fresh snow albedo (Wang et al. 2020). More need to be done in the future to quantify the influence of these physics.

However, snow cover in the permafrost regions of the QTP is thin, patchy, and short-lived (Che et al., 2019) because of the high wind speed (Yuan et al., 2016; Xie et al., 2019) and strong solar radiation (Meng et al., 2018). Its influence on soil temperature and contribution to permafrost state is usually considered weak (Jin et al., 2008). The in-situ measurements at TGL site also showed limited influence on soil temperature (Fig. 3), which is consistent with the studies at an alpine wetland site (Zhang et al., 2018) and the Yellow River source (Yao et al., 2019) on the QTP. The insufficient of numerical models for snow simulation seriously suppresses the accuracy of soil temperature (Fig. S1). For practical purpose, the snow processes is usually neglected when modeling the permafrost state in the QTP (Qin et al., 2017; Zou et al., 2017; Wu et al., 2018).

4.1 4.2   Possible reasons for the cold bias of soil temperature

The cold bias of soil temperature on the QTP are widely reported in many of the state-of-the-art LSMs (Yang et al., 2009;Chen et al., 2019). One of the main reason can be the inability of representing the diurnal variation of roughness length for heat (Z_{0h})

25

463 on the QTP (Yang et al., 2008; Chen et al., 2010), which is of great importance for a

464 reliable calculation of the sensible and latent heat, and thus for the soil surface/profile

465 temperature calculation (Zeng et al., 2012; Zheng et al., 2012). Noah-MP parameterize

466 Z_{0h} in the two schemes of SFC process (Table 1). In the M-O scheme, Z_{0h} is taken as

467 the same with the roughness length for momentum (Z_{0m}, Niu et al., 2011). The Chen97

468 scheme adopts the Zilitinkevitch approach (Zilitinkevich, 1995). However, both of

469 them couldn't produce the diurnal variation of $Z_{0,h}$ (Chen et al., 2010).

470   Another possible reason is the poor representation of the thermal conductivity (λ)

471 of frozen soil. Considering that the λ of ice is nearly four times higher than liquid

472 water, λ of frozen soil is generally expected to be greater than that of unfrozen soil.

473 Many parameterization schemes of λ, including the Johansen scheme in Noah-MP,

474 follow this pattern (Du et al., 2020). However, contrary phenomenon is widely reported

475 over the QTP (Pan et al., 2016; Hu et al., 2017; Yi et al., 2018; Li et al., 2019), including

476 the TGL site (Li et al., 2019). As a result, a majority of the state-of-the-art LSMs have

477 tended to overestimate the soil thermal conductivity of the QTP (Luo et al., 2009; Chen

478 et al., 2012; Du et al., 2020), which exactly explains the underestimation of soil

479 temperature during cold season and, at times, an overestimation during the warm season

480 (Luo et al., 2009).

481 **4.24.3   Discussions on the sensitivity of physical processes**

482 **4.23.1 Vegetation model (VEG) and canopy gap for radiation transfer (RAD)**

483   Noah-MP computes energy fluxes in vegetated fraction and bare fraction

484 separately and then sum them up weighted by vegetation fraction (FVEG). As list in

485 Table 1, VEG process includes three options to calculate the variation of vegetation

486 fraction (FVEG) FVEG in this study. VEG(3) calculates the daily FVEG based on the

487 interpolated LAI, while VEG(1) and VEG(4) uses the prescribed monthly and

488 maximum LAIFVEG, respectively. Obviously, VEG(3) produces more realistic FVEG

489 over the year, followed by VEG(1) and VEG(4). VEG(4) grossly overestimates the

490 FVEG, especially that during the cold season. Consequently, VEG(3) outperformed

26

491 VEG(1) and VEG(4). However, VEG(4) is widely used in many studies (Gao et al.,
492 2015; Chen et al., 2016; Li et al., 2018) despite overestimating the FVEG. In this study,
493 VEG(4) performed better than VEG(1).

494   RAD treats the radiation transfer process within the vegetation, and adopts three
495 methods to calculate the canopy gap. RAD(1) defines canopy gap as a function of the
496 3D vegetation structure and the solar zenith angle, RAD(2) employs no gap within
497 canopy, and RAD(3) treat the canopy gap from unity minus the FVEG (Niu and Yang,
498 2004). The RAD(3) scheme penetrates the most solar radiation to the ground, followed
499 by the RAD(1) and RAD(2) schemes. As an alpine grassland, there is a relative low
500 LAI at TGL site, and thus a quite high canopy gap. So, schemes with a larger canopy
501 gap could realistically reflect the environment. Consequently, the performance
502 decreased in the order of RAD(3) > RAD(1) > RAD(2) for ST/SLW simulation.

503 **4.~~2~~3.2 Canopy stomatal resistance (CRS) and soil moisture factor for stomatal**
504 **resistance (BTR)**

505   The biophysical process BTR and CRS directly affect the canopy stomatal
506 resistance and thus the plant transpiration (Niu et al., 2011). The transpiration of plants
507 could impact the ST through its cooling effect (Shen et al., 2015) and the water balance
508 of root zone (Chang et al., 2020). However, the annual transpiration of alpine steppe is
509 weak due to the shallow effective root zone and lower stomatal control in this dry
510 environment (Ma et al., 2015), which may explain the indistinctive or very small
511 difference among the schemes of the BTR and CRS processes (Fig. 7 and 8). ~~As a result,~~
512 ~~the BTR process was insensitive at all layers. CRS(1) and CRS(2) had no significant~~
513 ~~difference at most layers except the last two layers. However, the performance~~
514 ~~difference between CRS(1) and CRS(2) at the last two layers is very small (Fig. 3 and~~
515 ~~5).~~

516 **4.~~2~~3.3 Runoff and groundwater (RUN)**

517   For the RUN process, RUN(~~3~~2) had the worst performance for simulating ~~soil~~
518 ~~moisture (Fig. S1) and thus for~~ ST and SLW (Fig. ~~5~~7 and 8) among the four schemes,

likely due to its higher estimation of soil moisture (Fig. S6) and thus greater sensible heat and smaller ST (Gao et al., 2015). ~~free drainage assumption for subsurface runoff (Schaake et al., 1996), which is partly consistent with the study of Zhang et al. (2016) that RUN(3) is the worst-performing scheme for sensible and latent heat simulation in most cases compared with RUN(1) and RUN(2). RUN(4) also adopts the free drainage concept.~~ Consistent with the study of Li et al. (2015), RUN(3) performed the best at shallow layers for ST during the warm season, while that for SLW were less good. However, RUN(4) outperformed RUN(3) at deep layers, which may be explained by the better agreement of SLW by RUN(4) (Fig. 8 and S6). ~~It can be explained by the fourth power function of wetness at the top 2-m soil in RUN(4), in which the partition of surface runoff and infiltration is regulated by soil moisture (Yang and Dickinson, 1996).~~ Likewise, RUN(4) was on a par with RUN(1) in the simulation of ST due to the very small difference in SLW of two schemes (Fig. 8 and S6).~~unfrozen water (Fig. S1). Consequently, there was no or very small difference between RUN(4) and RUN(1) at shallow/deep soils (Fig. 5).~~ For the whole soil column, RUN(4) surpassed RUN(1) and RUN(2), both of which define surface/subsurface runoff as functions of groundwater table depth (Niu et al., 2005; Niu et al., 2007). This is in keeping with the study of Zheng et al. (2017) that soil water storage-based parameterizations outperform the groundwater table-based parameterizations in simulating the total runoff in a seasonally frozen and high-altitude Tibetan river, Besides, RUN(4) is designed based on the infiltration-excess runoff (Yang and Dickinson, 1996) in spite of the saturation-excess runoff in RUN(1) and RUN(2) (Gan et al., 2019), which is more common in arid and semiarid areas like the permafrost regions of QTP (Pilgrim et al., 1988).

4.~~2~~3.4 Surface layer drag coefficient (SFC)

SFC defines the calculations of the surface exchange coefficient for heat and water vapor (CH), which greatly impact the energy and water balance and thus the temperature and moisture of ~~land surface~~soil. SFC(1) adopts the Monin-Obukhov similarity theory (MOST) with a general form, while the SFC(2) uses the improved MOST modified by Chen et al. (1997). The most distinct difference between them is

548   that SFC(1) considers the zero-displacement height while SFC(2) parameterizes Z_{0h} and

549   Z_{0m} using different schemes. The difference between SFC(1) and SFC(2) has a great

550   impact on the CH value. Several studies have reported that SFC(2) has a better

551   performance for the simulation of sensible and latent heat on the QTP (Zhang et al.,

552   2016; Gan et al., 2019). The results of ~~Tukey's~~ T-test in this study showed remarkable

553   distinctions between the two schemes, where SFC(2) was dramatically superior to

554   SFC(1) (Fig. ~~5~~7 and 8). SFC(2) produces lower CH than SFC(1) (Zhang et al., 2014),

555   resulting in less efficient ventilation and greater heating of the land surface (Yang et al.,

556   2011b), and substantial improvement of the cold bias of Noah-MP in this study (Fig. 4).

557   As the sensible heat rising, the latent heat decline (Gao et al., 2015) and the dry bias of

558   Noah-MP is mitigated (Fig. 8).

4.~~2~~3.5 Super-cooled liquid water (FRZ) and frozen soil permeability (INF)

560   FRZ treats ~~unfrozen water~~liquid water ~~(super-cooled liquid water)~~ in frozen soil

561   (super-cooled liquid water) using two forms of freezing-point depression equation.

562   FRZ(1) takes a general form (Niu and Yang, 2006), while FRZ(2) exhibits a variant

563   form that considers the increased surface area of icy soil particles (Koren et al., 1999).

564   FRZ(2) generally yields more liquid water in comparison of FRZ(1). ~~In this study~~For

565   ST simulation, FRZ process did not show sensitivity at the shallow soil layers (5cm and

566   25cm) during the warm season (Fig. S2), but showed an increasing sensitivity at the

567   deep layers, especially during the cold season (Fig. ~~3~~4 and S3)~~,)~~. ~~which~~This can be

568   related to the greater sensitivity of FRZ (Fig. 4, S4 and S5) and the longer frozen

569   duration ~~of~~at deep soil and during the cold season.

570   INF(1) uses soil moisture (Niu and Yang, 2006) while INF(2) employs only the

571   liquid water (Koren et al., 1999) to parameterize soil hydraulic properties. INF(2)

572   generally produces more impermeable frozen soil than INF(1), which is also found in

573   this study (Fig. ~~S2~~S7). Due to the more realistic representation of ~~unfrozen water~~SLW

574   during the cold season (Fig. ~~S2~~S7), INF(2) surpassed INF(1) in simulating ST at 5 cm

575   ~~and 25 cm~~depth, while INF(1) outperformed INF(2) at 70 cm, 140 cm and 220 cm (Fig.

576   ~~5~~7). This result also indicate that INF(1) and INF(2) could alleviate the overestimation

and underestimation of ~~unfrozen water~~SLW, respectively. INF(2) ~~performed~~ simulated

worse ST than INF(1) at 300 cm depth (Fig. ~~5~~7) in spite of the better agreement with

~~unfrozen water~~observed SLW (Fig. ~~S2~~8 and S7), which may be related to the

overestimation of soil moisture of INF(2) at the depth of 140 cm.

4.~~2~~3.6 Lower boundary of soil temperature (TBOT) and snow/soil temperature

time scheme (STC)

TBOT process adopts two schemes to describe the soil temperature boundary

conditions. TBOT (1) assumes zero heat flux at the bottom of the model, while TBOT(2)

adopts the soil temperature at the 8 m depth (Yang et al., 2011a). In general, TBOT(1)

is expected to accumulate heat in the deep soil and produce higher ST than TBOT(2).

In this study, the two assumptions performed significantly different, especially at the

deep soil. Although TBOT(2) is more representative of the realistic condition, TBOT(1)

greatly surpassed TBOT(2) at the depth of 300cm~~in this study~~. It can be related to the

overall underestimation of the model, which can be alleviated by TBOT(1) because of

heat accumulation (Fig. ~~S3~~S8).

Two time discretization strategies are implemented in the STC process, where

STC(1) adopts the semi-implicit scheme while STC(2) uses the full implicit scheme, to

solve the thermal diffusion equation in first soil or snow layers (Yang et al., 2011a).

STC(1) and STC(2) are not strictly a physical processes but different upper boundary

conditions of soil column (You et al., 2019). The differences between STC(1) and

STC(2) were significant (Fig. ~~5~~7). Snow processes are not involved in this study, the

impacts of the two options on ST is remarkable (Fig. ~~5~~6), particularly in the shallow

layers and during the cold season (Fig. ~~3~~6). In addition, STC(2) outperformed STC(1)

in the ensemble ~~simulation experiments~~ simulated ST(Fig. ~~5~~7), because the higher ST

produced by STC(2) (Fig. ~~S4~~S9) alleviated the overall underestimation of Noah-MP.

4.~~3~~4.4   Perspectives

This study analyzed the characteristics and general behaviors of each

604 parameterization scheme of Noah-MP at a typical permafrost site on the QTP, hoping
605 to provide a reference for simulating permafrost state on the QTP. We identified the
606 systematic overestimation of snow cover and cold bias in Noah-MP, and discussed the
607 possible sources of error. Relevant results and methodologies can be practical
608 guidelines for improving the parameterizations of physical processes and testing their
609 uncertainties towards near-surface permafrost modeling on the plateau. Although the
610 site we selected may be representative for the typical environment on the plateau,
611 continued investigation with a broad spectrum of climate and environmental conditions
612 is required to make a general conclusion at regional scale.

613 ~~We identified the systematic cold bias of Noah-MP and discussed the possible~~
614 ~~sources of error, and analyzed the characteristics and general behavior of each~~
615 ~~parameterization scheme at a permafrost site on the QTP. This work would be~~
616 ~~constructive to a better understanding of the land surface processes on the QTP and~~
617 ~~further model improvements towards near-surface permafrost modeling using the~~
618 ~~LSMs.~~

619 ~~Although the optimal combination demonstrated in this study is only from the~~
620 ~~selected site, our results provide a practical way to investigate the permafrost state on~~
621 ~~the QTP. The optimal combination well simulated the ST, especially that of deep layers~~
622 ~~(Fig. 2). The representation of deep ST is crucial for permafrost modeling, which~~
623 ~~directly affects the permafrost features such as active layer thickness and temperature~~
624 ~~at the top of the permafrost. Further investigation with a broad spectrum of climate and~~
625 ~~environmental conditions is necessary to make a general conclusion.~~

5   Conclusions

627 In this study, an ensemble simulation ~~of soil temperature~~ using multi-
628 parameterizations was conducted using the Noah-MP model at the TGL site, aiming to
629 provide a reference for permafrost simulation using LSMs. The model was modified to
630 consider the vertical heterogeneity in the soil and the simulation depth was extended to
631 cover the whole active layer. The ensemble simulation consists of 6912

632 parameterization experiments, combining ten physical processes (VEG, CRS, BTR,

633 RUN, SFC, FRZ, INF, RAD, TBOT, and STC) each with multiple optional schemes.

634 On this basis, the general performance of Noah-MP was assessed by comparing

635 simulation results with in situ observations, and the sensitivity of soil temperature and

636 moisture at different depth of active layer to parameterization schemes was explored.

637 Furthermore, we proposed a new method to extract the optimal combination of schemes

638 to simulate soil temperature in the permafrost regions of the QTP. The main conclusions

639 are as follows:

640 (1) Noah-MP model tends to overestimate snow cover and thus largely underestimate

641   soil temperature in the permafrost regions of the QTP. Systematic cold bias and

642   large uncertainties of soil temperature still exist after removing the snow processes,

643   has relatively large uncertainties in the cold season, particularly at the deep layers

644   and during the cold season. Moreover, the model tends to underestimate soil

645   temperature, especially during the cold season. This is largely due to the imperfect

646   model structure with regard to the roughness length for heat and soil thermal

647   conductivity.

648 (2) Soil temperature is dominated by the surface layer drag coefficient (SFC) while

649   largely influenced by runoff and groundwater (RUN). SFC(2) and RUN(3) could

650   significantly alleviate and aggravate the cold bias of soil temperature, respectively.

651   Other physical processes have little impact on ST simulation, among which VEG,

652   RAD, and STC are more influential on shallow ST, while FRZ, INF and TBOT have

653   greater impacts on deep ST. In addition, CRS and BTR do not significantly affect

654   the simulation results.

655 (3) The best scheme combination for permafrost simulation are as follows: VEG (table

656   LAI, calculated vegetation fraction), CRS (Jarvis), BTR (Noah), RUN (BATS),

657   SFC (Chen97), RAD (zero canopy gap), FRZ (variant freezing-point depression),

658   INF (hydraulic parameters defined by soil moisture), TBOT (ST at 8 m), STC (semi-

659   implicit).

660

689   **References**

690   Benjamini, Y.: Simultaneous and selective inference: Current successes and future challenges,
691   Biometrical J., 52, 708-721, https://doi.org/10.1002/bimj.200900299, 2010.
692   Cao, B., Zhang, T., Wu, Q., Sheng, Y., Zhao, L., and Zou, D.: Brief communication: Evaluation and
693   inter-comparisons of Qinghai–Tibet Plateau permafrost maps based on a new inventory of field
694   evidence, The Cryosphere, 13, 511-519, https://doi.org/10.5194/tc-13-511-2019, 2019.
695   Chang, M., Liao, W., Wang, X., Zhang, Q., Chen, W., Wu, Z., and Hu, Z.: An optimal ensemble of
696   the Noah-MP land surface model for simulating surface heat fluxes over a typical subtropical
697   forest   in   South   China,   Agric.   For.   Meteor.,   281,   107815,
698   https://doi.org/https://doi.org/10.1016/j.agrformet.2019.107815, 2020.
699   Che, T., Hao, X., Dai, L., Li, H., Huang, X., and Xiao, L.: Snow cover variation and its impacts over
700   the   Qinghai-Tibet   Plateau,   Bull.   Chin.   Acad.   Sci.,   34,   1247-1253,
701   https://doi.org/10.16418/j.issn.1000-3045.2019.11.007, 2019.
702   Chen, F., Janjić, Z., and Mitchell, K.: Impact of atmospheric surface-layer parameterizations in the
703   new land-surface scheme of the NCEP Mesoscale Eta Model. Boundary-Layer Meteorol. 85, 391-
704   421, https://doi.org/10.1023/A:1000531001463, 1997.
705   Chen, L., Li, Y., Chen, F., Barr, A., Barlage, M., and Wan, B.: The incorporation of an organic soil
706   layer in the Noah-MP land surface model and its evaluation over a boreal aspen forest, Atmos.
707   Chem. Phys., 16, 8375-8387, https://doi.org/10.5194/acp-16-8375-2016, 2016.
708   Chen, R., Yang, M., Wang, X., and Wan, G.: Review on simulation of land-surface processes on the
709   Tibetan Plateau, Sci. Cold Arid Reg., 11, 93-115, https://doi.org/10.3724/SP.J.1226.2019.00093,
710   2019.
711   Chen, S., Li, X., Wu, T., Xue, K., Luo, D., Wang, X., Wu, Q., Kang, S., Zhou, H., and Wei, D.: Soil
712   thermal regime alteration under experimental warming in permafrost regions of the central
713   Tibetan   Plateau,   Geoderma,   372,   114397,
714   https://doi.org/https://doi.org/10.1016/j.geoderma.2020.114397, 2020.
715   Chen, Y., Yang, K., Zhou, D., Qin, J., and Guo, X.: Improving the Noah Land Surface Model in Arid
716   Regions with an Appropriate Parameterization of the Thermal Roughness Length, J.
717   Hydrometeor., 11, 995-1006, https://doi.org/10.1175/2010JHM1185.1, 2010.
718   Chen, Y., Yang, K., Tang, W., Qin, J., and Zhao, L.: Parameterizing soil organic carbon's impacts
719   on soil porosity and thermal parameters for Eastern Tibet grasslands, Sci. Chin. Earth Sci., 55,
720   1001-1011, https://doi.org/10.1007/s11430-012-4433-0, 2012.
721   Claverie, M., Matthews, J. L., Vermote, E. F., and Justice, C. O.: A 30+ Year AVHRR LAI and
722   FAPAR Climate Data Record: Algorithm Description and Validation, Remote Sens., 8, 263,
723   https://doi.org/10.3390/rs8030263, 2016.
724   Cosby, B. J., Hornberger, G. M., Clapp, R. B., and Ginn, T. R.: A Statistical Exploration of the
725   Relationships of Soil Moisture Characteristics to the Physical Properties of Soils, Water Resour.
726   Res., 20, 682-690, https://doi.org/10.1029/WR020i006p00682, 1984.
727   Daniel, R., Nikolay, S., Bernd, E., Stephan, G., and Sergei, M.: Recent advances in permafrost
728   modelling, Permafr. Periglac. Process., 19, 137-156, https://doi.org/doi:10.1002/ppp.615, 2008.
729   Du, Y., Li, R., Zhao, L., Yang, C., Wu, T., Hu, G., Xiao, Y., Zhu, X., Yang, S., Ni, J., and Ma, J.:
730   Evaluation of 11 soil thermal conductivity schemes for the permafrost region of the central

731   Qinghai-Tibet   Plateau,   CATENA,   193,   104608,
732   https://doi.org/https://doi.org/10.1016/j.catena.2020.104608, 2020.

733 Fountain, A. G., Campbell, J. L., Schuur, E. A. G., Stammerjohn, S. E., Williams, M. W., and
734   Ducklow, H. W.: The Disappearing Cryosphere: Impacts and Ecosystem Responses to Rapid
735   Cryosphere Loss, BioScience, 62, 405-415, https://doi.org/10.1525/bio.2012.62.4.11, 2012.

736 Gan, Y. J., Liang, X. Z., Duan, Q. Y., Chen, F., Li, J. D., and Zhang, Y.: Assessment and Reduction
737   of the Physical Parameterization Uncertainty for Noah-MP Land Surface Model, Water Resour.
738   Res., 55, 5518-5538, https://doi.org/10.1029/2019wr024814, 2019.

739 Gao, Y., Kai, L., Fei, C., Jiang, Y., and Lu, C.: Assessing and improving Noah-MP land model
740   simulations for the central Tibetan Plateau, J. Geophys. Res.-Atmos., 120, 9258-9278, 2015.

741 Guo, D., and Wang, H.: Simulation of permafrost and seasonally frozen ground conditions on the
742   Tibetan   Plateau,   1981-2010,   J.   Geophys.   Res.-Atmos.,   118,   5216-5230,
743   https://doi.org/10.1002/jgrd.50457, 2013.

744 He, K., Sun, J., and Chen, Q.: Response of climate and soil texture to net primary productivity and
745   precipitation-use efficiency in the Tibetan Plateau, Pratacultural Science, 36, 1053–1065.
746   https://doi.org/10.11829/j.issn.1001-0629.2019-0036, 2019.

747 Hillel, D.: Applications of Soil Physics, Academic Press, 400 pp., 1980.

748 Hjort, J., Karjalainen, O., Aalto, J., Westermann, S., Romanovsky, V. E., Nelson, F. E., Etzelmüller,
749   B., and Luoto, M.: Degrading permafrost puts Arctic infrastructure at risk by mid-century, Nat.
750   Commun., 9, 5147, https://doi.org/10.1038/s41467-018-07557-4, 2018.

751 Hong, S., Yu, X., Park, S. K., Choi, Y. S., and Myoung, B.: Assessing optimal set of implemented
752   physical parameterization schemes in a multi-physics land surface model using genetic algorithm,
753   Geosci. Model Dev., 7, 2517-2529, https://doi.org/10.5194/gmd-7-2517-2014, 2014.

754 Hu, G., Zhao, L., Li, R., Wu, T., Wu, X., Pang, Q., Xiao, Y., Qiao, Y., and Shi, J.: Modeling
755   hydrothermal transfer processes in permafrost regions of Qinghai-Tibet Plateau in China, Chin.
756   Geograph. Sci., 25, 713-727, https://doi.org/10.1007/s11769-015-0733-6, 2015.

757 Hu, G., Zhao, L., Wu, X., Li, R., Wu, T., Xie, C., Pang, Q., and Zou, D.: Comparison of the thermal
758   conductivity parameterizations for a freeze-thaw algorithm with a multi-layered soil in permafrost
759   regions, Catena, 156, 244-251, https://doi.org/10.1016/j.catena.2017.04.011, 2017.

760 Jiang, Y., Chen, F., Gao, Y., He, C., Barlage, M., and Huang, W.: Assessment of uncertainty sources
761   in snow cover simulation in the Tibetan Plateau, J. Geophys. Res.-Atmos., 125, e2020JD032674,
762   https://doi.org/10.1029/2020JD032674, 2020.

763 Jin, H., Sun, L., Wang, S., He, R., Lu, L., and Yu, S.: Dual influences of local environmentalVariables
764   on ground temperatures on the interior-eastern Qinghai-Tibet Plateau (I): vegetation and snow
765   cover. J. Glaciol. Geocryol. 30, 535–545, 2008.

766 Koren, V., Schaake, J., Mitchell, K., Duan, Q. Y., Chen, F., and Baker, J. M.: A parameterization of
767   snowpack and frozen ground intended for NCEP weather and climate models, J. Geophys. Res.-
768   Atmos., 104, 19569-19585, https://doi.org/10.1029/1999JD900232, 1999.

769 Koven, C., Riley, W., and Stern, A.: Analysis of Permafrost Thermal Dynamics and Response to
770   Climate   Change   in   the   CMIP5   Earth   System   Models,   J.   Clim.,   26,   1877-1900,
771   https://doi.org/10.1175/JCLI-D-12-00228.1, 2013.

772 Lawrence, D., Fisher, R., Koven, C., Oleson, K., Swenson, S., Vertenstein, M.: Technical description
773   of version 5.0 of the Community Land Model (CLM), Boulder, Colorado, 2018.

774 Li, J., Chen, F., Zhang, G., Barlage, M., Gan, Y., Xin, Y., and Wang, C.: Impacts of Land Cover and

Soil Texture Uncertainty on Land Model Simulations Over the Central Tibetan Plateau, J. Adv. Model. Earth Sy., 10, 2121-2146, https://doi.org/10.1029/2018ms001377, 2018.

Li, K., Gao, Y., Fei, C., Xu, J., Jiang, Y., Xiao, L., Li, R., and Pan, Y.: Simulation of impact of roots on soil moisture and surface fluxes over central Qinghai−Xizang Plateau. Plateau Meteor., 34, 642-652, https://doi.org/10.7522/j.issn.1000-0534.2015.00035, 2015.

Li, R., Zhao, L., Wu, T., Wang, Q. X., Ding, Y., Yao, J., Wu, X., Hu, G., Xiao, Y., Du, Y., Zhu, X., Qin, Y., Shuhua, Y., Bai, R., Erji, D., Liu, G., Zou, D., Yongping, Q., and Shi, J.: Soil thermal conductivity and its influencing factors at the Tanggula permafrost region on the Qinghai–Tibet Plateau, Agric. For. Meteor., 264, 235-246, https://doi.org/10.1016/j.agrformet.2018.10.011, 2019.

Li, X., Wu, T., Zhu, X., Jiang, Y., Hu, G., Hao, J., Ni, J., Li, R., Qiao, Y., Yang, C., Ma, W., Wen, A., and Ying, X.: Improving the Noah-MP Model for simulating hydrothermal regime of the active layer in the permafrost regions of the Qinghai-Tibet Plateau, J. Geophys. Res.-Atmos., 125, e2020JD032588, https://doi.org/10.1029/2020JD032588, 2020.

Luo, D., Wu, Q., Jin, H., Marchenko, S., Lyu, L., and Gao, S.: Recent changes in the active layer thickness across the northern hemisphere, Environ. Earth Sci., 75, 555. https://doi.org/10.1007/s12665-015-5229-2, 2016.

Luo, S., Lyu, S., Zhang, Y., Hu, Z., Ma, Y. M., Li, S. S., and Shang, L.: Soil thermal conductivity parameterization establishment and application in numerical model of central Tibetan Plateau, Chin. J. Geophys., 52, 919-928, https://doi.org/10.3969/j.issn.0001-5733.2009.04.008, 2009.

Ma, N., Zhang, Y., Guo, Y., Gao, H., Zhang, H., and Wang, Y.: Environmental and biophysical controls on the evapotranspiration over the highest alpine steppe, J. Hydrol., 529, 980-992, https://doi.org/https://doi.org/10.1016/j.jhydrol.2015.09.013, 2015.

Maheu, A., Anctil, F., Gaborit, É., Fortin, V., Nadeau, D. F., and Therrien, R.: A field evaluation of soil moisture modelling with the Soil, Vegetation, and Snow (SVS) land surface model using evapotranspiration observations as forcing data, J. Hydrol., 558, 532-545, https://doi.org/https://doi.org/10.1016/j.jhydrol.2018.01.065, 2018.

Melton, J., Verseghy, D., Sospedra-Alfonso, R., and Gruber, S.: Improving permafrost physics in the coupled Canadian Land Surface Scheme (v.3.6.2) and Canadian Terrestrial Ecosystem Model (v.2.1) (CLASS-CTEM), Geosci. Model Dev., 12, 4443-4467, https://doi.org/10.5194/gmd-12-4443-2019, 2019.

Nicolsky, D. J., Romanovsky, V. E., Alexeev, V. A., and Lawrence, D. M.: Improved modeling of permafrost dynamics in a GCM land-surface scheme, Geophys. Res. Lett., 34, L08501, https://doi.org/10.1029/2007gl029525, 2007.

Niu, G.-Y., and Yang, Z.-L.: Effects of vegetation canopy processes on snow surface energy and mass balances, J. Geophys. Res.-Atmos., 109, D23111, https://doi.org/10.1029/2004jd004884, 2004.

Niu, G.-Y., and Yang, Z.-L.: Effects of Frozen Soil on Snowmelt Runoff and Soil Water Storage at a Continental Scale, J. Hydrometeor., 7, 937-952, https://doi.org/10.1175/JHM538.1, 2006.

Niu, G.-Y., Yang, Z.-L., Dickinson, R. E., and Gulden, L. E.: A simple TOPMODEL-based runoff parameterization (SIMTOP) for use in global climate models, J. Geophys. Res.-Atmos., 110, D21106, https://doi.org/10.1029/2005jd006111, 2005.

Niu, G.-Y., Yang, Z.-L., Dickinson, R. E., Gulden, L. E., and Su, H.: Development of a simple groundwater model for use in climate models and evaluation with Gravity Recovery and Climate

819   Experiment data, J. Geophys. Res.-Atmos., 112, D07103, https://doi.org/10.1029/2006jd007522,
820   2007.

821   Niu, G.-Y., Yang, Z.-L., Mitchell, K. E., Chen, F., Ek, M. B., Barlage, M., Kumar, A., Manning, K.,
822   Niyogi, D., and Rosero, E.: The community Noah land surface model with multiparameterization
823   options (Noah-MP): 1. Model description and evaluation with local-scale measurements, J.
824   Geophys. Res.-Atmos., 116, D12109, https://doi.org/10.1029/2010JD015139, 2011.

825   Pan, X., Li, Y., Yu, Q., Shi, X., Yang, D., and Roth, K.: Effects of stratified active layers on high-
826   altitude permafrost warming: a case study on the Qinghai–Tibet Plateau, The Cryosphere, 10,
827   1591-1603, https://doi.org/10.5194/tc-10-1591-2016, 2016.

828   Park, S., and Park, S.K.: Parameterization of the snow-covered surface albedo in the Noah-MP
829   Version 1.0 by implementing vegetation effects, Geosci. Model Dev. 9, 1073-1085,
830   https://doi.org/10.5194/gmd-9-1073-2016, 2016.

831   Pilgrim, D. H., Chapman, T. G., and Doran, D. G.: Problems of rainfall-runoff modelling in arid and
832   semiarid regions, Hydrolog. Sci. J., 33, 379-400, https://doi.org/10.1080/02626668809491261,
833   1988.

834   Qin, Y., Wu, T., Zhao, L., Wu, X., Li, R., Xie, C., Pang, Q., Hu, G., Qiao, Y., Zhao, G., Liu, G., Zhu,
835   X., and Hao, J.: Numerical modeling of the active layer thickness and permafrost thermal state
836   across Qinghai-Tibetan Plateau. J. Geophys. Res.-Atmos., 122, 11,604-611,620,
837   https://doi.org/10.1002/2017JD026858, 2017.

838   Ran, Y., Xin, L., and Cheng, G.: Climate warming over the past half century has led to thermal
839   degradation of permafrost on the Qinghai–Tibet Plateau, Cryosphere, 12, 595-608,
840   https://doi.org/10.5194/tc-12-595-2018, 2018.

841   Schaake, J. C., Koren, V. I., Duan, Q. Y., Mitchell, K., and Chen, F.: Simple water balance model
842   for estimating runoff at different spatial and temporal scales, J. Geophys. Res.-Atmos., 101, 7461-
843   7475, https://doi.org/10.1029/95jd02892, 1996.

844   Shen, M., Piao, S., Jeong, S.-J., Zhou, L., Zeng, Z., Ciais, P., Chen, D., Huang, M., Jin, C.-S., Li, L.
845   Z. X., Li, Y., Myneni, R. B., Yang, K., Zhang, G., Zhang, Y., and Yao, T.: Evaporative cooling
846   over the Tibetan Plateau induced by vegetation growth, Proc. Natl. Acad. Sci. U. S. A., 112, 9299-
847   9304, https://doi.org/10.1073/pnas.1504418112, 2015.

848   Wang, W., Yang, K., Zhao, L., Zheng, Z., Lu, H., Mamtimin, A., Ding, B., Li, X., Zhao, L., Li, H.,
849   Che, T., and Moore, J. C.: Characterizing Surface Albedo of Shallow Fresh Snow and Its
850   Importance for Snow Ablation on the Interior of the Tibetan Plateau, J. Hydrometeor., 21, 815-
851   827, https://doi.org/10.1175/JHM-D-19-0193.1, 2020.

852   Wei, Z., and Dong, W.: Assessment of Simulations of Snow Depth in the Qinghai-Tibetan Plateau
853   Using CMIP5 Multi-Models, Arct. Antarct. Alp. Res., 47, 611-525,
854   https://doi.org/10.1657/AAAR0014-050, 2015.

855   Westermann, S., Langer, M., Boike, J., Heikenfeld, M., Peter, M., Etzelmuller, B., and Krinner, G.:
856   Simulating the thermal regime and thaw processes of ice-rich permafrost ground with the land-
857   surface model CryoGrid 3, Geosci. Model Dev., 9, 523-546, https://doi.org/10.5194/gmd-9-523-
858   2016, 2016.

859   Wetzel, P., and Chang, J.-T.: Concerning the Relationship between Evapotranspiration and Soil
860   Moisture, J. Clim. Appl. Meteorol., 26, 18-27, https://doi.org/10.1175/1520-
861   0450(1987)026<0018:CTRBEA>2.0.CO;2, 1987.

862   Woo, M. K.: Permafrost Hydrology, Springer, Berlin, Heidelberg, 2012.

Wu, X., and Nan, Z.: A multilayer soil texture dataset for permafrost modeling over Qinghai-Tibetan Plateau. Paper presented at 2016 IEEE International Geoscience and Remote Sensing Symposium (IGARSS), Beijing, China. https://doi.org/10.1109/IGARSS.2016.7730283, 2016.

Wu, X. B., Nan, Z. T., Zhao, S. P., Zhao, L., and Cheng, G. D.: Spatial modeling of permafrost distribution and properties on the Qinghai-Tibet Plateau, Permafr. Periglac. Process., 29, 86-99, https://doi.org/10.1002/ppp.1971, 2018.

Xie, Z., Hu, Z., Ma, Y., Sun, G., Gu, L., Liu, S., Wang, Y., Zheng, H., and Ma, W.: Modeling blowing snow over the Tibetan Plateau with the community land model: Method and preliminary evaluation, J. Geophys. Res.-Atmos., 124, 9332–9355, https://doi.org/10.1029/2019jd030684, 2019.

Yang, K., Koike, T., Ye, B., and Bastidas, L.: Inverse analysis of the role of soil vertical heterogeneity in controlling surface soil state and energy partition, J. Geophys. Res.-Atmos., 110, D08101, https://doi.org/10.1029/2004jd005500, 2005.

Yang, K., Koike, T., Ishikawa, H., Kim, J., Li, X., Liu, H., Shaomin, L., Ma, Y., and Wang, J.: Turbulent Flux Transfer over Bare-Soil Surfaces: Characteristics and Parameterization, J. Appl. Meteorol. Clim., 47, 276-290, https://doi.org/10.1175/2007JAMC1547.1, 2008.

Yang, K., Chen, Y. Y., and Qin, J.: Some practical notes on the land surface modeling in the Tibetan Plateau, Hydrol. Earth Syst. Sci., 13, 687-701, https://doi.org/10.5194/hess-13-687-2009, 2009.

Yang, Z.-L., and Dickinson, R. E.: Description of the biosphere-atmosphere transfer scheme (BATS) for the soil moisture workshop and evaluation of its performance, Global Planet. Change, 13, 117-134, https://doi.org/10.1016/0921-8181(95)00041-0, 1996.

Yang, Z.-L., Cai, X., Zhang, G., Tavakoly, A., Jin, Q., Meyer, L., and Guan, X.: The Community Noah Land Surface Model with Multi-Parameterization Options (Noah-MP): Technical Description, 2011a.

Yang, Z.-L., Niu, G.-Y., E. Mitchell, K., Chen, F., B. Ek, M., Barlage, M., Longuevergne, L., Manning, K., Niyogi, D., Tewari, M., and Xia, Y.: The community Noah land surface model with multiparameterization options (Noah-MP): 2. Evaluation over global river basins. J. Geophys. Res.-Atmos. 116, D12110, https://doi.org/10.1029/2010JD015140, 2011b.

Yao, C., Lyu, S., Wang, T., Wang, J., and Ma, C.: Analysis on freezing-thawing characteristics of soil in high and low snowfall years in source region of the Yellow River, Plateau Meteor., 38, 474-483, 2019.

Yao, J., Zhao, L., Gu, L., Qiao, Y., and Jiao, K.: The surface energy budget in the permafrost region of the Tibetan Plateau, Atmos. Res., 102, 394-407, https://doi.org/https://doi.org/10.1016/j.atmosres.2011.09.001, 2011.

Yi, S., Zhou, Z., Ren, S., Ming, X., Yu, Q., Shengyun, C., and Baisheng, Y.: Effects of permafrost degradation on alpine grassland in a semi-arid basin on the Qinghai–Tibetan Plateau, Environ. Res. Lett., 6, 045403, https://doi.org/10.1088/1748-9326/6/4/045403, 2011.

Yi, S., He, Y., Guo, X., Chen, J., Wu, Q., Qin, Y., and Ding, Y.: The physical properties of coarse-fragment soils and their effects on permafrost dynamics: a case study on the central Qinghai–Tibetan Plateau, The Cryosphere, 12, 3067-3083, https://doi.org/10.5194/tc-12-3067-2018, 2018.

You, Y. H., Huang, C. L., Yang, Z. L., Zhang, Y., Bai, Y. L., and Gu, J.: Assessing Noah-MP Parameterization Sensitivity and Uncertainty Interval Across Snow Climates, J. Geophys. Res.-Atmos., 125, e2019JD030417, https://doi.org/10.1029/2019jd030417, 2020.

Yuan, W., Xu, W., Ma, M., Chen, S., Liu, W., and Cui, L.: Improved snow cover model in terrestrial

ecosystem models over the Qinghai–Tibetan Plateau, Agric. For. Meteor., 218-219, 161-170, https://doi.org/10.1016/j.agrformet.2015.12.004, 2016.

Zeng, X., Wang, Z., and Wang, A.: Surface Skin Temperature and the Interplay between Sensible and Ground Heat Fluxes over Arid Regions, J. Hydrometeor., 13, 1359-1370, https://doi.org/10.1175/JHM-D-11-0117.1, 2012.

Zhang, G., Chen, F., and Gan, Y.: Assessing uncertainties in the Noah-MP ensemble simulations of a cropland site during the Tibet Joint International Cooperation program field campaign, J. Geophys. Res.-Atmos., 121, 9576-9596, https://doi.org/10.1002/2016jd024928, 2016.

Zhang, H., Su. Y., Jiang, H., Chao, H., and Su, W.: Influence of snow subliming process on land-atmosphere interaction at alpine wetland, J. Glaci. Geocry., 40, 1223-1230, 2018.

Zhang, T.: Influence of the seasonal snow cover on the ground thermal regime: An overview, Reviews of Geophysics, 43, RG4002, https://doi.org/10.1029/2004RG000157, 2005.

Zhao, L., Hu, G., Zou, D., Wu, X., Ma, L., Sun, Z., Yuan, L., Zhou, H., and Liu, S.: Permafrost changes and its effects on hydrological processes on Qinghai-Tibet Plateau, Bull. Chin. Acad. Sci., 34, 1233-1246, https://doi.org/10.16418/j.issn.1000-3045.2019.11.006, 2019.

Zheng, D., Van Der Velde, R., Su, Z., Wen, J., and Wang, X.: Assessment of Noah land surface model with various runoff parameterizations over a Tibetan river, J. Geophys. Res.-Atmos., 122, 1488-1504, https://doi.org/10.1002/2016jd025572, 2017.

Zheng, H., Yang, Z.-L., Lin, P., Wei, J., Wu, W.-Y., Li, L., Zhao, L., and Wang, S.: On the sensitivity of the precipitation partitioning into evapotranspiration and runoff in land surface parameterizations, Water Resour. Res., 55, 95-111, https://doi.org/10.1029/2017WR022236, 2019.

Zheng, W., Wei, H., Wang, Z., Zeng, X., Meng, J., Ek, M., Mitchell, K., and Derber, J.: Improvement of daytime land surface skin temperature over arid regions in the NCEP GFS model and its impact on satellite data assimilation, J. Geophys. Res.-Atmos., 117, D06117, https://doi.org/10.1029/2011jd015901, 2012.

Zilitinkevich, S.: Non-local turbulent transport pollution dispersion aspects of coherent structure of convective flows, Air Pollution III, Air pollution theory and simulation (H Power, N Moussiopoulos, C A Brebbia, eds) Computational Mechanics Publ , Southampton, Boston, 1, 53-60, 1995.

Zou, D., Zhao, L., Sheng, Y., Chen, J., Hu, G., Wu, T., Wu, J., Xie, C., Wu, X., Pang, Q., Wang, W., Du, E., Li, W., Liu, G., Li, J., Qin, Y., Qiao, Y., Wang, Z., Shi, J., and Cheng, G.: A new map of permafrost distribution on the Tibetan Plateau, The Cryosphere, 11, 2527-2542, https://doi.org/10.5194/tc-11-2527-2017, 2017.

Supplement of

Assessing the simulated soil thermal regime from Noah-MP LSM v1.1 for near-surface permafrost modeling on the Qinghai-Tibet Plateau

Xiangfei Li et al.

Correspondence to: Tonghua Wu (thuawu@lzb.ac.cn)

Content: Equations S1-S7; Table S1; Figures S1-S4S9

The soil hydraulic parameters of each layer, including the porosity (θ_s), saturated hydraulic conductivity (K_s), hydraulic potential (ψ_s), the Clapp-Hornberger parameter (b), field capacity (θ_{ref}), wilt point (θ_w), and saturated soil water diffusivity (D_s), were determined using the pedotransfer functions proposed by Hillel (1980), Cosby et al. (1984), and Wetzel and Chang (1987):

$$\theta_s = 0.489 - 0.00126(\%sand) \tag{S1}$$

$$K_s = 7.0556 \times 10^{-6.884+0.0153(\%sand)} \tag{S2}$$

$$\psi_s = -0.01 \times 10^{1.88-0.0131(\%sand)} \tag{S3}$$

$$b = 2.91 + 0.159(\%clay) \tag{S4}$$

$$\theta_{ref} = \theta_s \left[\frac{1}{3} + \frac{2}{3}\left(\frac{5.79\times10^{-9}}{K_s}\right)^{1/(2b+3)} \right] \tag{S5}$$

$$\theta_w = 0.5\theta_s \left(\frac{-200}{\psi_s}\right)^{-1/b} \tag{S6}$$

$$D_s = b \cdot K_s \cdot \left(\frac{\psi_s}{\theta_s}\right) \tag{S7}$$

where %$sand$ and %$clay$ represent the percentage (%) of sand and clay content in soil, respectively.

Table S1 Soil discretization scheme and soil particle fraction in this study.

Layer	Z_i	ΔZ_i	$Z_{h,i}$	Sand (%)	Silt (%)	Clay (%)
1	0.010	0.020	0.020			
2	0.040	0.040	0.060	85.48	12.59	1.93
3	0.090	0.060	0.120			
4	0.160	0.080	0.200	83.51	13.57	2.92
5	0.260	0.120	0.320	81.15	15.58	3.27
6	0.400	0.160	0.480	86.62	11.16	2.22
7	0.580	0.200	0.680	78.73	18.06	3.21
8	0.800	0.240	0.920	88.12	8.98	2.90
9	1.060	0.280	1.200	95.00	3.00	2.00
10	1.360	0.320	1.520			
11	1.700	0.360	1.880	92.50	4.00	3.50
12	2.080	0.400	2.280	90.00	5.00	5.00
13	2.500	0.440	2.720			
14	2.990	0.540	3.260			
15	3.580	0.640	3.900			
16	4.270	0.740	4.640	68.00	20.00	12.00
17	5.060	0.840	5.480			
18	5.950	0.940	6.420			
19	6.940	1.040	7.460			
20	7.980	1.040	8.500			

Layer node depth (Z_i), thickness (ΔZ_i), and depth at layer interface ($Z_{h,i}$) for default soil column. All in meters.

Figure. S1. Monthly soil temperature (ST) at (a) 5 cm, (b) 25 cm, (c) 70 cm, (d) 140 cm, (e) 220 cm, (f) 300 cm at TGL site for observation (Obs), ensemble simulation considering snow (Sim-with snow), and ensemble simulation neglecting snow (Sim-no snow). The green and blue shadow represent the standard deviation of Sim-with snow and Sim-no snow experiments, respectively.
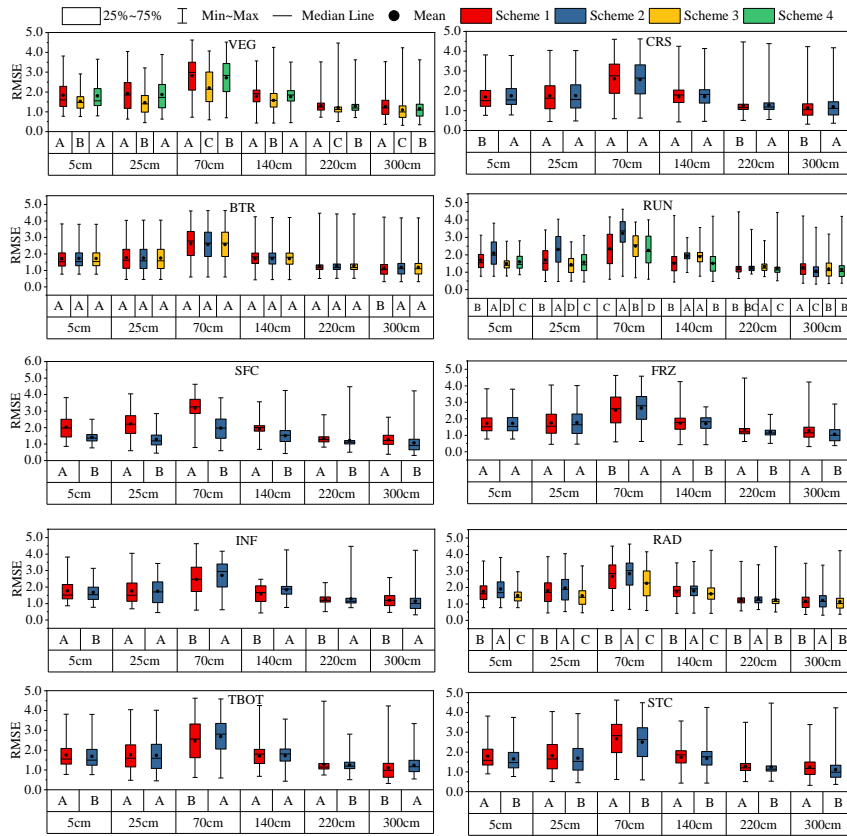
Figure S2. Distinction level for RMSE of ST at different layers during the warm season in the ensemble simulations. Limits of the boxes represent upper and lower quartiles, whiskers extend to the maximum and minimum RMSE. The black stations in the box are the average values. The lines in the box indicate the median value.
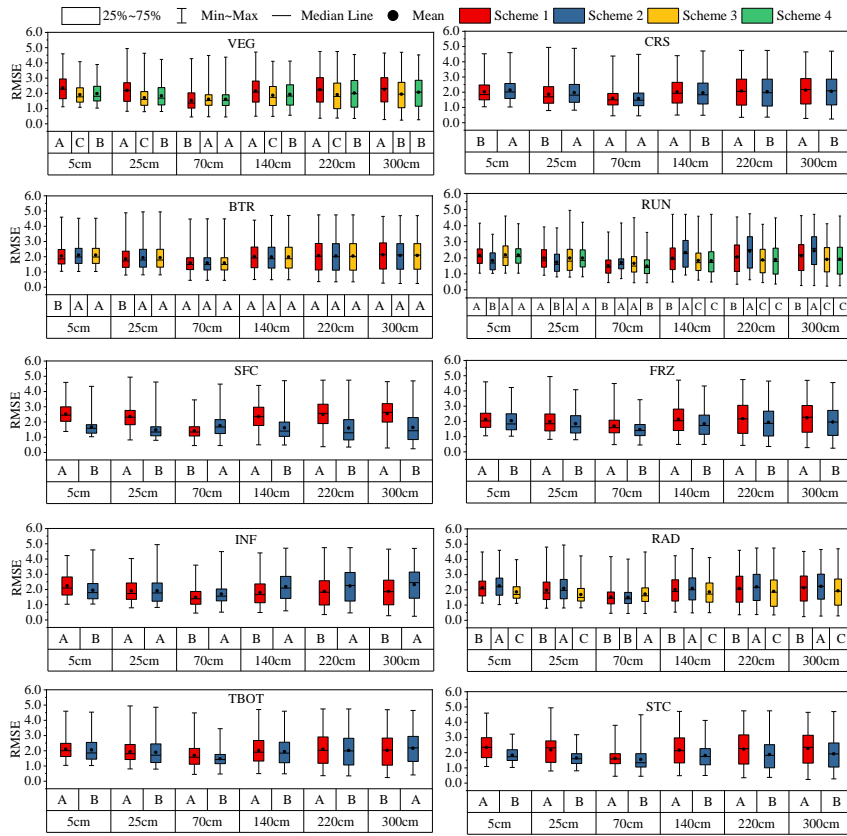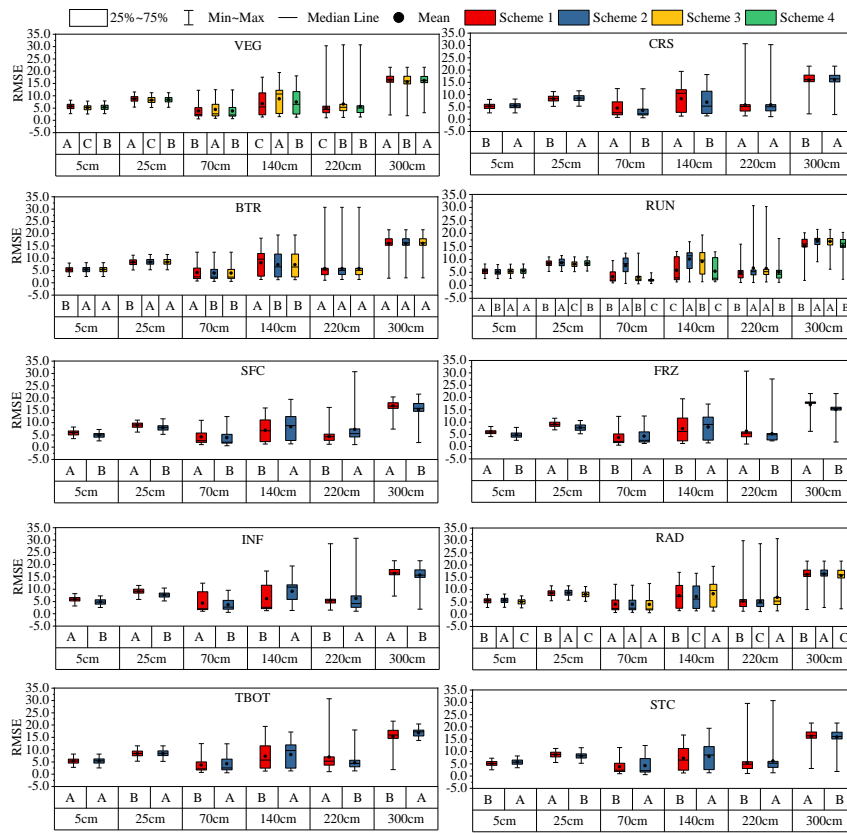
Figure S3. Distinction level for RMSE of ST at different layers during the cold season in the ensemble simulations. Limits of the boxes represent upper and lower quartiles, whiskers extend to the maximum and minimum RMSE. The black stations in the box are the average values. The lines in the box indicate the median value.
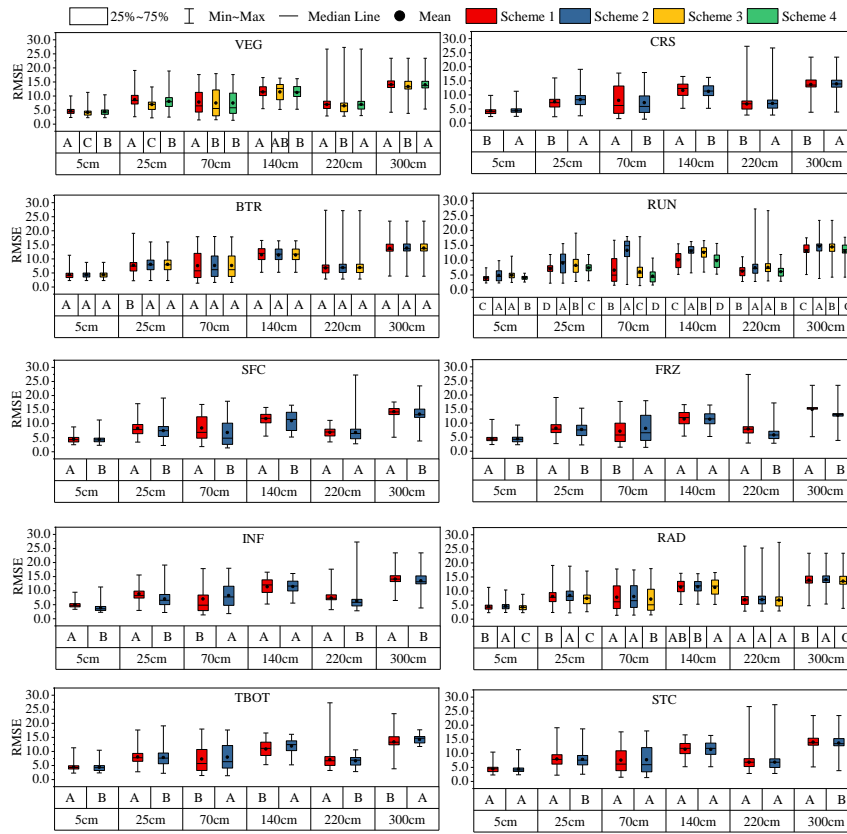
Figure S4. Distinction level for RMSE of SLW at different layers during the warm season in the ensemble simulations. Limits of the boxes represent upper and lower quartiles, whiskers extend to the maximum and minimum RMSE. The black stations in the box are the average values. The lines in the box indicate the median value.

Figure S5. Distinction level for RMSE of SLW at different layers during the cold season in the ensemble simulations. Limits of the boxes represent upper and lower quartiles, whiskers extend to the maximum and minimum RMSE. The black stations in the box are the average values. The lines in the box indicate the median value.
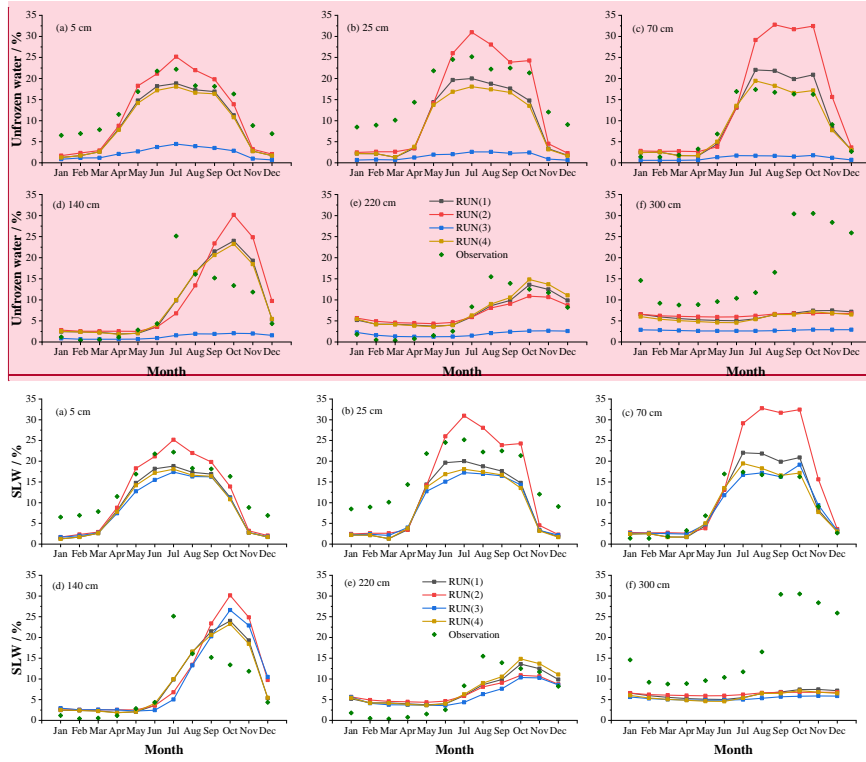
批注 [LX1]: deleted

Figure. ~~S1~~ S6 Monthly ~~unfrozen~~ soil liquid water (SLW in %) at (a) 5 cm, (b) 25 cm, (c) 70 cm, (d) 140 cm, (e) 220 cm, (f) 300 cm for the RUN process.
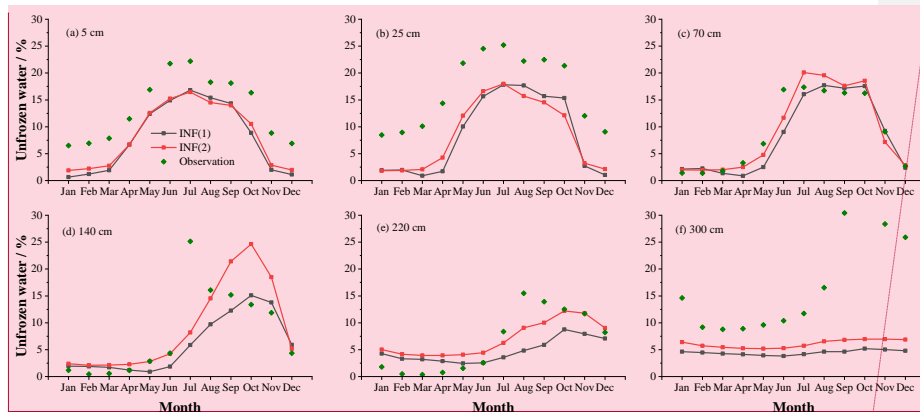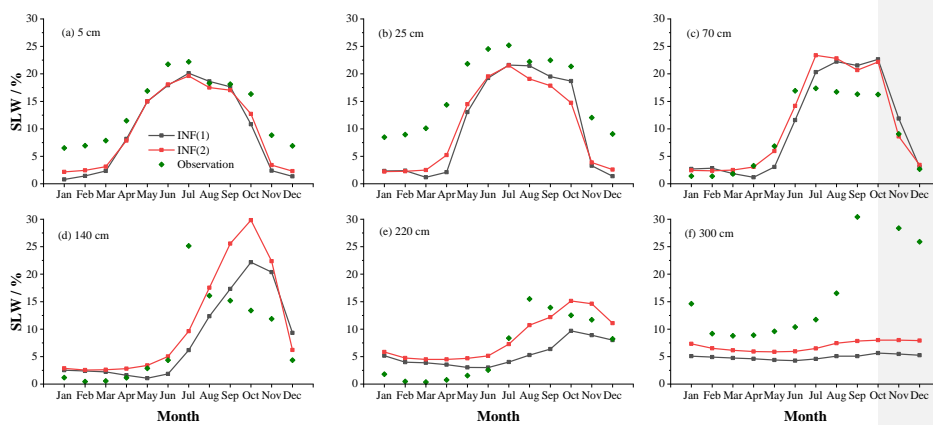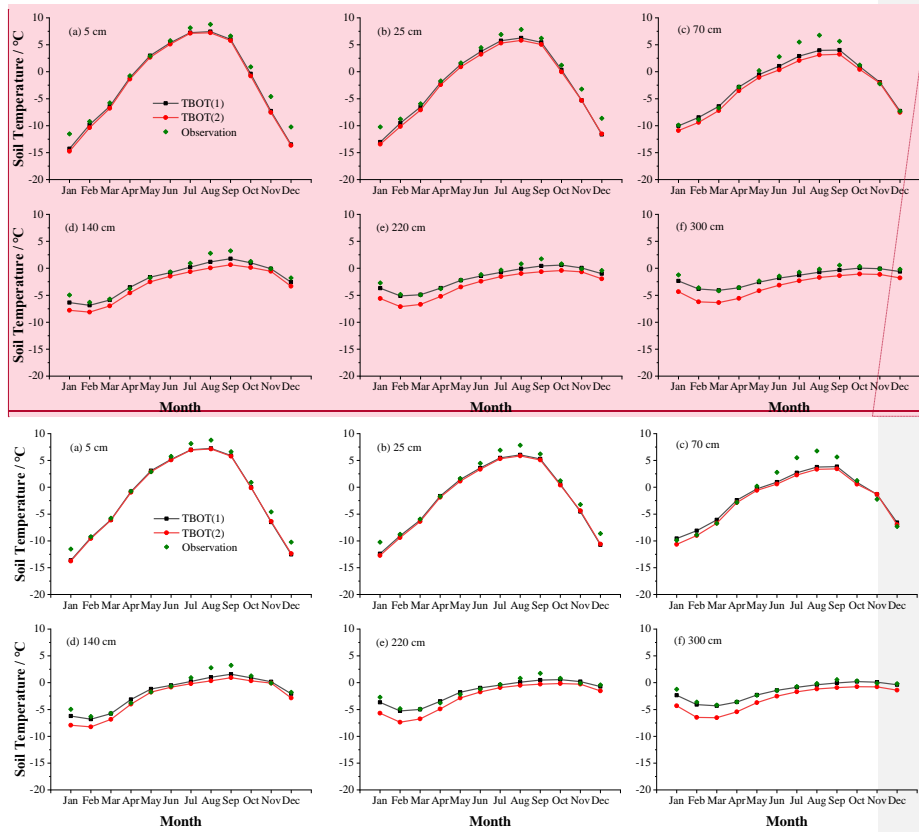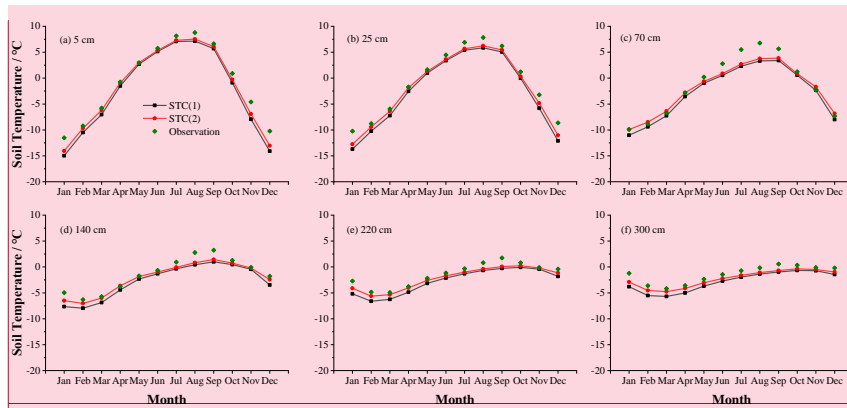
Figure. ~~S2~~ S7 Monthly ~~unfrozen~~ soil liquid water (SLW in %) at (a) 5 cm, (b) 25 cm, (c) 70 cm, (d) 140 cm, (e) 220 cm, (f) 300 cm for the INF process.

Figure. ~~S3~~ S8 Monthly soil temperature at (a) 5 cm, (b) 25 cm, (c) 70 cm, (d) 140 cm, (e) 220 cm, (f) 300 cm for the TBOT process.

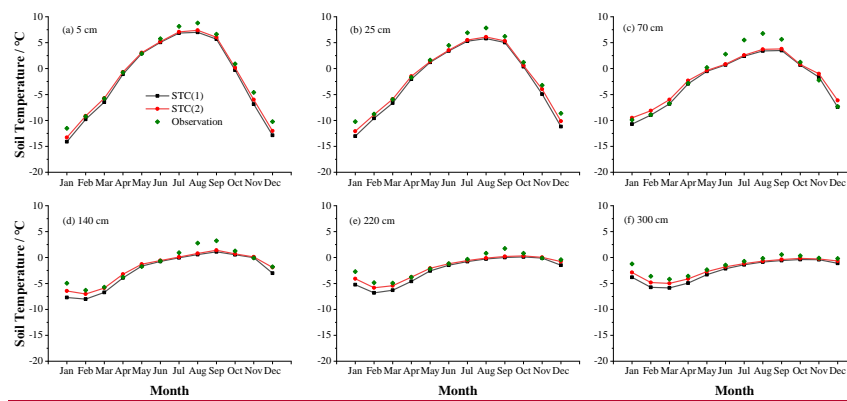**Figure.** ~~S4~~ S9 Monthly soil temperature at (a) 5 cm, (b) 25 cm, (c) 70 cm, (d) 140 cm, (e) 220 cm, (f) 300 cm for the STC process.

References:

Hillel, D.: Applications of Soil Physics, Academic Press, 400 pp., 1980.

Cosby, B. J., Hornberger, G. M., Clapp, R. B., and Ginn, T. R.: A Statistical Exploration of the Relationships of Soil Moisture Characteristics to the Physical Properties of Soils, Water Resour. Res., 20, 682-690, https://doi.org/10.1029/WR020i006p00682, 1984.

Wetzel, P., and Chang, J.-T.: Concerning the Relationship between Evapotranspiration and Soil Moisture, J. Clim. Appl. Meteorol., 26, 18-27, https://doi.org/10.1175/1520-0450(1987)026<0018:CTRBEA>2.0.CO;2, 1987.